Science Advances
AAAS

补充材料
Supplementary Materials for

废物中的稀土元素
Rare earth elements from waste

邓，王欣，邓，王哲，
Bing Deng, Xin Wang, Duy Xuan Luong, Robert A. Carter, Zhe Wang,
梅森·B·汤姆森，詹姆斯·M·图尔*
Mason B. Tomson, James M. Tour*

*通讯作者。 电子邮件：tour@rice.edu
*Corresponding author. Email: tour@rice.edu

2022年2月9日出版，Sci. Adv.8，eabm3132（2022）DOI:10.1126/sciadv.abm3132
Published 9 February 2022, *Sci. Adv.* **8**, eabm3132 (2022)
DOI: 10.1126/sciadv.abm3132

此PDF文件包括：
This PDF file includes:

补充文本

Supplementary Text

补充文本1。回收率的计算。

Supplementary Text 1. Calculation of the recovery yield.

CFA原料ctotal(CFA raw)中的总稀土含量是通过使用HF:HNO3消解方法的总消解来测量的(详见材料和方法，图S6)。

The total REE contents in CFA raw materials, c_{total}(CFA-Raw), was measured by total digestion using a HF:HNO_3 digestion method (see details in Materials and Methods, fig. S6). 通过对CFA原料进行HCl或HNO3浸出，测定了CFA原料c0(CFA原料)中可酸浸出的稀土元素含量。The acid-leachable REE contents in CFA raw materials, c_0(CFA-Raw), were measured by HCl or HNO_3 leaching of the CFA raw materials. CFA原料酸浸的稀土回收率由公式S1计算，The REE recovery yield by acid leaching the CFA raw materials was calculated by Eq. S1,

0=0(CFA原始)

$$Y_0 = \frac{c_0(\text{CFA-Raw})}{c_{\text{total}}(\text{CFA-Raw})} \quad \text{(S1)}$$

将CFA原料和炭黑混合并进行FJH活化过程。The CFA raw materials and carbon black were mixed and underwent the FJH activation process. 获得的固体称为活化CFA。The obtained solid is termed as activated CFA. 活化CFA c(活化CFA)中的可酸浸稀土含量在FJH后通过与CFA相同的酸浸程序进行测量。The acid-leachable REE content in the activated CFA, c(activated CFA), was measured by the same acid leaching procedure of CFA after FJH. 活化CFA酸浸的稀土回收率由等式S2计算，The REE recovery yield by acid leaching the activated CFA was calculated by Eq. S2,

=(激活的CFA)

$$Y = \frac{c(\text{activated CFA})}{c_{\text{total}}(\text{CFA-Raw})} \quad \text{(S2)}$$

因此，Y/Y0的比率由等式S3计算，Hence, the ratio of Y/Y_0 was calculated by Eq. S3,

=(激活的CFA)

$$\frac{Y}{Y_0} = \frac{c(\text{activated CFA})}{c_0(\text{CFA-Raw})} \quad \text{(S3)}$$

Y/Y0可作为通过FJH活化过程提高CFA稀土回收率的指标。The Y/Y_0 could be used as an index of the increase of the REE recovery yield from CFA by the FJH activation process. 如果Y/Y0>1，则活化过程具有积极影响并提高回收率。If $Y/Y_0 > 1$, the activation process has a positive effect and improves the recovery yield. 类似地，对于BR和电子废物，通过使用等式S4和等式S5计算回收率的增加：Similarly, for BR and e-waste, the increase of recovery yield is calculated by using Eq. S4 and Eq. S5:

=(已激活BR)

$$\frac{Y}{Y_0} = \frac{c(\text{activated BR})}{c_0(\text{BR-Raw})} \quad \text{(S4)}$$

=(活化e废物)

$$\frac{Y}{Y_0} = \frac{c(\text{activated e-waste})}{c_0(\text{e-waste-Raw})} \quad \text{(S5)}$$

0(e废物原料)

补充文本2。扩大FJH流程的策略。

Supplementary Text 2. Strategy for scaling up the FJH process.

焦耳加热广泛应用于许多设备和工业过程，如电加热器和管式炉。Joule heating is widely used in many devices and industrial processes, such as electric heaters and tube furnace. 本文报道的闪光焦耳加热(FJH)本质上是一个焦耳加热过程。Flash Joule heating (FJH) reported here, is intrinsically a Joule heating process. 对于传统的焦耳加热过程，使用恒定的长时间交流电(AC)或直流电(DC)作为电源。For traditional Joule heating process, a constant and long-time alternating current (AC) or direct current (DC) is used as the electrical resources. 相比之下，在我们小组首次发明的用于合成涡轮层状石墨烯(24)的FJH工艺中，使用了由电容器放电提供的脉冲直流电，其在短时间内提供了更高的温度。In contrast, in the FJH process, which is firstly invented by our group for the synthesis of turbostratic graphene (*24*), a pulsed DC provided by the discharging of capacitors is used, which provides a much higher temperature in a short duration. 本文对FJH过程进行了理论分析，以确定决定温度的关键参数；然后，我们通过实验证明了FJH过程是可扩展的。The FJH process is scalable. We here conduct theoretical analysis of the FJH process to identify the key parameters determining the temperature; then, we experimentally demonstrate the scaling-up of the FJH process; 我们还提供了连续生产的概念原型；最后，我们简要介绍了FJH工艺在石墨烯合成中正在进行的工业规模应用，该工艺可以很容易地用于稀土元素回收。we also provide conceptual prototype of the continuous production; lastly, we briefly mention the ongoing industrial scale application of the FJH process on graphene synthesis, which can be easily shifted for the REE recovery purpose.

标度规则的理论分析。

Theoretical analysis of the scaling rule.

对于放大，当样品质量增加时，保持恒定的温度值和温度分布至关重要。For scaling up, it is critical to maintain a constant temperature value and temperature distribution when the sample mass is increased.

通过等式S6计算焦耳加热产生的热量(Q)，The heat amount (Q) produced by Joule heating is calculated by Eq. S6,

$$Q = I^2 Rt \quad \text{(S6)}$$

其中I是通过样品的电流，R是样品电阻，t是时间。
where I is the current passing through the sample, R is the sample resistance, and t is the time.
考虑到单位体积热量(Qv)，可以将等式修改为等式S7，
Considering heat amount per volume (Q_v), the equation could be revised to Eq. S7,
v=2 e(S7)，其中Qv是每体积的热量，j是电流密度，e是样品的电阻率。

$$Q_v = j^2 \rho_e t \quad \text{(S7)}$$

where Q_v is the heat per volume, j is the current density, and ρ_e is the resistivity of the sample.
根据传热公式，可通过等式S8计算温度变化，
According to the heat transfer formula, the change of temperature could be calculated by Eq. S8,
=p(S8)，其中ΔT是温度变化，m是样品质量，Cp是比热容。

$$Q = C_p m \Delta T \quad \text{(S8)}$$

where ΔT is the change of temperature, m is the mass of the sample, and C_p is the specific heat capacity. Since the specific capacity (C_p) is a constant for a specific type of sample, the change of temperature is determined by the heat amount.
由于特定类型样品的比容量(Cp)是一个常数，因此温度变化由热量决定。
此外，我们可以将每体积的公式S8修改为公式S9，
Furthermore, we can revise the Eq. S8 per volume to Eq. S9,
v=p m(S9)，其中m是样品的密度。

$$Q_v = C_p \rho_m \Delta T \quad \text{(S9)}$$

where ρ_m is the density of the sample. Since the density (ρ_m) and the specific heat capacity (C_p) are constant for the sample, the change of temperature is linearly proportional to Q_v. In other word, regardless of the sample mass, the same temperature could be achieved as long as the Q_v remains the same.
由于样品的密度(m)和比热容(Cp)恒定，温度变化与Qv成线性比例。换句话说，无论样品质量如何，只要Qv保持不变，就可以实现相同的温度。
然后，根据等式S7，由于样品的电阻率(e)对于样品是恒定的，为了在放大样品质量(m)时保持恒定的Qv和t，我们需要保持恒定的j，其由等式S10确定，
Then, according to Eq. S7, since the resistivity (ρ_e) of the sample is constant for the sample, to keep a constant Q_v and t when scaling up the sample mass (m), we need to maintain a constant j, which is determined by Eq. S10,

$$j = \frac{I}{S} \quad \text{(S10)}$$

其中I是通过样品的电流，S是横截面积。
where I is the current passing through the sample, and S is the cross-sectional area. 电流由等式S11计算，The current is calculated by Eq. S11,

$$I = \frac{q}{t} \quad \text{(S11)}$$

其中q是电荷，t是时间。
where q is the charge, and t is the time.
假设电容器组中的电荷在t时间内放电，可以通过等式S12计算电荷，
Supposing that the charges in the capacitor bank are discharged within the time of t, the charge could be calculated by Eq. S12,
=(S12)，其中C是电容器组的总电容，V是充电电压。

$$q = CV \quad \text{(S12)}$$

where C is the total capacitance of the capacitor bank, and V is the charging voltage.
根据等式S10至12，电流密度由等式S13确定，
According to Eq. S10 to 12, the current density is determined by Eq. S13,

$$j = \frac{CV}{St} \quad \text{(S13)}$$

由于我们始终使用石英管，因此样品通常为圆柱形，因此样品质量通过等式S14计算，
The sample is usually cylinder-shaped since we always use a quartz tube, so the sample mass is calculated by Eq. S14,
=m(S14)，其中S是横截面积，L是样品长度。

$$m = \rho_m S L \quad \text{(S14)}$$

where S is the cross-sectional area, and L is the sample length.
根据等式S13和S14，通过等式S15确定电流密度
According to Eq. S13 and S14, the current density is determined by Eq. S15

$$j = \frac{CV\rho_m L}{mt} \quad \text{(S15)}$$

样品的密度(m)是恒定的，我们可以改变样品的横截面积以保持恒定的样品长度L。因此，当样品的质量(m)增加时，为了保持恒定的j和t，有两种方法：(1)增加焦耳加热电压V；和/或(2)增加C的电容。
The density of the sample (ρ_m) is constant, and we can change the sample cross-sectional area to maintain a constant sample length of L. Hence, to maintain a constant j and t when the mass (m) of the sample is increased, there are two approaches: (1) to increase the Joule heating voltage V; and/or (2) to increase the capacitance of C.

放大演示。
Scaling up demonstration.
我们在这里演示了通过使用第一种策略，增加电压来放大FJH过程。
We here demonstrated the scaling up of the FJH process by using the first strategy, increasing the voltage. 在大多数样品质量为m0=0.2 g的实验(表S1)中，我们使用FJH电压V0=120 V，电容C0=60 mF，以及圆柱形样品
In most of the experiments (table S1) with the sample mass of m_0 = 0.2 g, we use a FJH voltage of V_0 = 120 V and capacitance of C_0 = 60 mF, and a cylinder-shape sample

直径D0=8 mm（S0～50 mm2）。为了将反应放大到m1=2 g，我们使用了直径为D1=16 mm（S1 ~ 200 mm2）的大样本量。根据等式S14至S15，大规模样品的电压应为V1=2.5×V0=300 V。

with diameter of D_0 = 8 mm (S_0 ~ 50 mm^2). To scale up the reaction to m_1 = 2 g, we used a large sample size with diameter of D_1 = 16 mm (S_1 ~ 200 mm^2). According to Eq. S14 to S15, the voltage for the large-scale sample should be V_1 = 2.5 × V_0 = 300 V. We used CFA-C as an example and demonstrated the FJH process with mass up to 2 g (fig. S16A). The reaction conditions are: m_1 = 2 g, D_1 = 16 mm, V_1 = 300 V, and t = 1 s. The result is shown in fig. S16B. The CFA-C is successfully activated with the increase of REE recovery yields to 150% to 190%, comparable to the results of the sample with smaller mass (Fig. 2H).

我们以CFA-C为例，演示了质量高达2g的FJH过程（图S16A）。反应条件为：m1=2g，D1=16mm，V1=300V，t=1s。结果如图S16B所示。CFA-C被成功激活，REE回收率增加到150%-190%，与质量较小的样品的结果相当（图2H）。

我们还可以通过增加电容（C）来扩大FJH过程。在本研究中使用的第一代FJH系统中，电容器组由10个商用铝电解电容器组成，总电容为C0=60 mF。我们还在实验室建立了第二代FJH系统，总电容C2=0.624F。通过使用V2=380 V的FJH电压和C2=0.624 F的电容，我们实现了每批m2=5 g的样品质量。实际上，我们的实验室已经将煤转化为石墨烯的FJH工艺规模扩大到每天17.6公斤左右。由于石墨烯合成的主要FJH工艺和稀土元素回收的主要FJH工艺基本相同，因此可以安全地假设，在我们的研究实验室中，用于稀土元素回收的FJH工艺的生产率大于10 kg day-1。

We can also scale up the FJH process by increasing the capacitance (C). In our first generation FJH system, which is used in this work, the capacitor bank is composed of 10 commercial aluminum electrolytic capacitor and has a total capacitance of C_0 = 60 mF. We also built a second generation FJH system in our lab with the total capacitance of C_2 = 0.624 F. By using a FJH voltage of V_2 =380 V and capacitance of C_2 = 0.624 F, we realized the sample mass of m_2 = 5 g per batch. Actually, our lab has already scaled the FJH process for the conversion of coal to graphene to ~17.6 kg day^{-1}. Since the main FJH process for graphene synthesis and for REE recovery is pretty the same, it is safe to presume that the FJH process for REE recovery has the production rate of >10 kg day^{-1} in our research lab.

连续生产的概念原型。

The conceptual prototype of the continuous production.

在我们目前的工作中，FJH过程是分批进行的。我们假设FJH过程可以连续自动完成，正如我们在石墨烯生产过程中所证明的那样。我们在此提供了连续生产反应器的概念原型（图S17）。连续生产过程包括四个步骤。CFA/CB原料的混合物被装载到传送带上的腔室中。将样品压缩至特定电阻。然后样品进行FJH反应。最后，收集活化的CFA产物。这只是一种可能的设计。考虑到各种商业上可用的连续生产工艺和设备，如滚带工艺，我们的FJH工艺可以整合到其中，以回收稀土元素。

In our present work, the FJH process is done batch-by-batch. We presume that the FJH process could be done automatically in a continuous manner as we have demonstrated in our graphene production process. We provide here a conceptual prototype of the continuous production reactor (fig. S17). The continuous production process consists of four steps. The mixture of CFA/CB feedstock is loaded onto the chamber on the conveyor belt. The sample is compressed to a specific resistance. The sample then undergoes the FJH reaction. Lastly, the activated CFA product is collected. This is only one possible design. Considering the various commercially available continuous production processes and equipment, such as rolling-belt processes, our FJH process could be integrated into them for the purpose of REE recovery.

FJH工艺的商业规模正在扩大。

The commercial scaling up of the FJH process is ongoing.

环球物质股份有限公司正在将FJH工艺应用于石墨烯的工业规模生产(https://www.universalmatter.com/)到2022年第二季度，目标产量为每天1吨，到2023年，进一步扩大到每天100吨。到目前为止，生产率每9周翻一番。为石墨烯生产设计和优化的设备和工艺可用于稀土元素回收。在工业规模上，交流电（AC）比直流电（DC）更可行。根据我们的上述分析，优化电压是扩大FJH工艺的一种方法。在工业上，高达数百kV的高压甚至超高压是成熟的技术，可以应用于REE工艺。因此，FJH过程为REE恢复的可扩展性提供了一条可行的途径。FJH工艺正在进行的商业规模化为今后从大规模废物中回收稀土元素铺平了道路。

The application of the FJH process to an industrial scale for the production of graphene is ongoing by Universal Matter Inc. (https://www.universalmatter.com/), with the targeted production rate of 1 ton day^{-1} by Q2 2022, and further scaling to 100 tons per day by 2023. To date, the production rate doubles every 9 weeks. The equipment and process designed and optimized for graphene production could be applied for REE recovery purpose. At the industrial scale, alternative current (AC) is a more feasible electrical resource than the direct current (DC). According to our above analysis, optimizing the voltage is one approach to scale up the FJH process. In industry, the high voltage or even ultrahigh voltage up to hundreds of kV are mature technologies, which could be applied in the REE process. Hence, the FJH process has a tried route to scalability for the REE recovery. The ongoing commercial scaling of the FJH process paves the way for future REE recovery from large-scale waste products.

补充文本3。能耗计算和利润估算。

Supplementary Text 3. Energy consumption calculation and profit estimation.

电能(E)消耗通过等式S16计算，

The electrical energy (E) consumption is calculated by Eq. S16,

$$E = \frac{(V_1^2 - V_2^2) \times C}{2 \times M} \quad \text{(S16)}$$

其中V1和V2分别是FJH后的起始电压和结束电压，C是电容(60 mF)，M是每批的质量。

where V_1 and V_2 are the start voltage and the end voltage after the FJH, respectively, C is the capacitance (60 mF), and M is the mass per batch.

在V1=120 V、V2=0 V、C=60 mF和M=0.2 g的典型实验中，能量计算为E=2.16 kJ g-1=6.0×10-4 kWh g-1=600 kWh ton-1

In a typical experiment with V_1 = 120 V, V_2 = 0 V, C = 60 mF, and M = 0.2 g, the energy is calculated to be,

E = 2.16 kJ g^{-1} = 6.0 × 10^{-4} kWh g^{-1} = 600 kWh ton^{-1}

考虑到美国德克萨斯州的工业电价为0.02 kWh-1美元，激活1吨CFA的成本将为P(电力)=12$ton-1。

Considering that the industrial electricity price in Texas, USA is \$0.02 kWh^{-1}, the cost for activating 1 ton of CFA would be P(electricity) = 12 \$ ton^{-1}.

与未经活化过程的稀土元素回收相比，通过活化过程增加的回收稀土量可通过等式S17计算，

Compared with the REE recovery without the activation process, the increased recovered REE amount by the activation process could be calculated by Eq. S17,

=××(S17)其中m是稀土元素的质量，m是CFA原料的质量，c是CFA原料中稀土元素的可提取含量，ΔY是热活化过程后提高的稀土回收率。

$$m = M \times c \times \Delta Y \quad \text{(S17)}$$

where m is the mass of the REE, M is the mass of CFA raw materials, c is the extractable content of REE from CFA raw materials, and ΔY is the improved REE recovery yield after the thermal activation process.

对于从CFA中回收稀土元素，Sc和临界稀土元素，包括Nd、Eu、Dy、Er和Tb，贡献了80%以上的值(4)。

For REE recovery from CFA, the Sc, and critical REE, including Nd, Eu, Dy, Er, and Tb, contribute to more than 80% of the values (*4*). 考虑到1吨CFA-C，改进后的回收REE量为：m(Sc)=23 g，m(Nd)=29 g，m(Eu)=2 g，m(Dy)=5 g，m(Er)=3 g，m(Tb)=3 g Considering 1 ton of CFA-C, the improved recovered REE amount would be:

m(Sc) = 23 g, m(Nd) = 29 g, m(Eu) = 2 g, m(Dy) = 5 g, m(Er) = 3 g, and m(Tb) = 3 g

2019年7月，这些关键稀土元素的价格为Sc(P=5735 kg-1)、Nd(P=64 kg-1)、Eu(P=285 kg-1)、Dy(P=375 kg-1)、Er(P=30 kg-1)和Tb(P=770 kg-1)(53)。单个稀土元素的值为：P(Sc)=$132，P(Nd)=$1.8，P(Eu)=$0.6，P(Dy)=$1.9，P(Er)=$0.1，P(Tb)=$2.3

The price of these critical REE are Sc (P = \$5735 kg^{-1}), Nd (P = \$64 kg^{-1}), Eu (P = \$285 kg^{-1}), Dy (P = \$375 kg^{-1}), Er (P = \$30 kg^{-1}), and Tb (P = \$770 kg^{-1}) in July 2019 (*53*). The values of the individual REE would be:

P(Sc) = \$132, P(Nd) = \$1.8, P(Eu) = \$0.6, P(Dy) = \$1.9, P(Er) = \$0.1, and P(Tb) = \$2.3

采用热活化工艺的稀土元素的附加值为：P(REE)=139吨-1美元

The value added of the REEs with the thermal activation process would be:

P(REE) = \$139 ton^{-1}

在这里，我们假设直接浸出过程和活化浸出过程的稀土分离成本是恒定的。

Here, we presume that the REE separation cost is constant for the directly leaching process and the activation-leaching process. 激活过程的利润百分比由等式S18计算，The profit percentage for the activation process is calculated by Eq. S18,

利润百分比=(REE)(电力)

$$\text{Profit percentage} = \frac{P(\text{REE}) - P(\text{electricity})}{P(\text{electricity})} \quad \text{(S18)}$$

经计算，利润率约为11%。考虑到其他稀土元素回收率的提高，利润率可能会更大。

The profit percentage is calculated to be ~11. The profit margin could be larger considering the improved recovery of other REE.

补充文本4。 渗滤液中的杂质及其去除设想。

Supplementary Text 4. The impurities in the leachate and the envision on impurity removal.

稀土元素分离通常分为一级分离(稀土元素与其他杂质元素的分离)和二级分离(单个稀土元素的分离)(54)。

REE separation is generally classified as primary separation (the separation of REE from other impurity elements), and secondary separation (the separation of individual REE) (*54*). 含稀土元素的渗滤液中金属杂质的存在会通过溶剂萃取和离子交换等方法影响后续稀土元素分离效率(51、54、55)。 The presence of metal impurities in the REE-containing leachate affects the subsequent REE separation efficiency by methods such as solvent extraction and ion exchange (*51*, *54*, *55*). 因此，通常需要在稀土元素分离之前去除杂质(54)。 Hence, the impurities usually need to be removed prior to the REE separation (*54*). 在这里，分析了渗滤液中的杂质，并设想从渗滤液中去除金属杂质和选择性分离单个稀土元素。 Here, the impurities in the leachate are analyzed, and the removal of metal impurities and selective separation of individual REE from the leachate are envisioned.

渗滤液中的杂质。

The impurities in the leachate.

矿石和二次废物的成分通常因来源不同而显著不同，因此渗滤液中的杂质在类型和含量上也存在显著差异(54)。

The composition of ores and secondary wastes often differ significantly from one source to another, and hence the impurities in the leachate also vary significantly in types and contents (*54*). 主要杂质包括Al、Si、Fe、Ca、Mg、Zn、Co、Ni、Cr、Cu等。杂质，尤其是杂质含量与稀土含量的比率，可能通过与稀土元素共沉淀、消耗试剂、乳化等方式影响稀土元素的回收和沉淀效率(54，55)。 The major impurities include Al, Si, Fe, Ca, Mg, Zn, Co, Ni, Cr, Cu, *etc*. Impurities, and especially the ratio of impurity content to REE content, could affect REE recovery and precipitation efficiencies by co-precipitation with REE, consuming the reagents, emulsification, *etc*. (*54*, *55*). 在这里，我们测量了来自不同二次资源的稀土浸出液中的杂质含量。 Here, we measured the impurity contents in our REE leachates from different secondary resources.

对于CFA-F，主要杂质包括铝、硅、铁、钙(10至100 ppm)、镁(1至10 ppm)、锌、镍、铬(0.1至1 ppm)和钴(0.01至0.1 ppm)(图S18)。 For CFA-F, the major impurities include Al, Si, Fe, Ca (10 to 100 ppm), Mg (1 to 10 ppm), Zn, Ni, Cr (0.1 to 1 ppm), and Co (0.01 to 0.1 ppm) (fig. S18). 我们发现，在0到2的所有测试pH条件下，活化CFA-F的c(REE)/c(杂质)比CFA-F原料的c(REE)/c(杂质)比都要大(图S18D)。 We found that ratio of *c*(REE)/*c*(Impurity) for the activated CFA-F is larger than that of the CFA-F raw materials for all the tested pH conditions ranging from 0 to 2 (fig. S18D). 这意味着FJH工艺有助于提高稀土元素的浸出能力，同时在一定程度上降低CFA-F的杂质浸出能力，这有利于杂质去除。 This means that the FJH process helps to increase the REE leachability while to some extent reduce the impurity leachability from CFA-F, which is beneficial for impurity removal. 对于CFA-C，主要杂质包括铝、硅(>100 ppm)、铁、钙、镁(10至100 ppm)、锌(1至10 ppm)、镍、铬(0.1至1 ppm)和钴(0.01至0.1 ppm)(图S19)。 For CFA-C, the major impurities include Al, Si (>100 ppm), Fe, Ca, Mg (10 to 100 ppm), Zn (1 to 10 ppm), Ni, Cr (0.1 to 1 ppm), and Co (0.01 to 0.1 ppm) (fig. S19). 类似地，当测试pH值为0和1时，活化CFA-c的c(REE)/c(杂质)比CFA-c原料的c(REE)/c(杂质)比更大(图S19C)。 Similarly, the ratio of *c*(REE)/*c*(Impurity) for the activated CFA-C is larger than that of the CFA-C raw materials for the tested pH of 0 and 1 (fig. S19C).

对于溴，主要杂质包括铝、铁(>100 ppm)、硅、钙(10至100 ppm)、镁、镍、铬、铜(1至10 ppm)、锌(0.1至1 ppm)和钴(0.01至0.1 ppm)(图S20A)。 For BR, the major impurities include Al, Fe (>100 ppm), Si, Ca (10 to 100 ppm), Mg, Ni, Cr, Cu (1 to 10 ppm), Zn (0.1 to 1 ppm), and Co (0.01 to 0.1 ppm) (fig. S20A). BR原料的c(REE)/c(杂质)比率大于活化BR的比率(图S20B)。 The ratio of *c*(REE)/*c*(Impurity) for the BR raw materials is larger than that of the activated BR (fig. S20B). 这意味着FJH还提高了杂质浸出能力，尤其是Fe(图S20A)。 This means that the FJH also enhances the impurity leachability, especially Fe (fig. S20A). 对于e-waste，主要杂质包括Cu(>100 ppm)、Al、Si、Fe、Zn(10至100 ppm)、Ca、Mg、Ni(1至10 ppm)以及Co和Cr(0.1至1 ppm)(图S20C)。 For e-waste, the major impurities include Cu (>100 ppm), Al, Si, Fe, Zn (10 to 100 ppm), Ca, Mg, Ni (1 to 10 ppm), and Co and Cr (0.1 to 1 ppm) (fig. S20C). 活化电子废物的c(REE)/c(杂质)比率大于电子废物原料的比率(图S20D)。 The ratio of *c*(REE)/*c*(Impurity) for the activated e-waste is larger than that of the e-waste raw materials (fig. S20D).

上述杂质分析将有助于设计合适的下游稀土元素净化和分离工艺。

The above impurity analysis would be helpful for the design of appropriate downstream REE purification and separation processing. 通过调整浸出条件(例如矿浆密度、pH值、酸类型、温度、时间等)，可以进一步优化杂质含量和杂质与稀土元素的比例。 The impurities content and the ratio of impurities to REE could be further optimized by adjusting the leaching conditions (*e.g.*, pulp density, pH, acid type, temperature, time, *etc*.).

讨论从浸出液中去除杂质的可能性。

Discussion on possible removal of impurities from the leach liquors.

许多技术，包括溶剂萃取、离子交换或吸附以及选择性沉淀，已广泛用于去除浸出液中的杂质(54)。

Many techniques, including solvent extraction, ion exchange or adsorption, and selective precipitation, have been widely used to remove the impurities in leach liquor (*54*). 适用路线在很大程度上取决于杂质类型和含量以及稀土元素的目标应用。 The applicable route significantly depends on the impurities type and content, and the target application of REE. 在我们从CFA或BR获得的浸出液中，主要杂质为浓度>10 ppm的铝、硅、铁、镁和钙，而从ewaste获得的浸出液也应考虑铜和锌。 In our leach liquor obtained from CFA or BR, the major impurities are Al, Si, Fe, Mg, and Ca with concentration >10 ppm, while Cu and Zn should also be considered for the leach liquor from e-waste. 许多方法已广泛用于去除这些杂质(54)。 Many methods have already been widely used for removing these impurities (*54*). 例如，对于含铁溶液，酸性萃取剂，例如二-(2-乙基己基)磷酸 For example, for the Fe-containing solution, acidic extractants such as di-(2-ethylhexyl)phosphoric

酸(D2EHPA)可以在适当的萃取剂浓度和有机/水比(56)下选择性地萃取稀土元素。
acid (D2EHPA) can selectively extract REE with appropriate extractant concentration and organic/aqueous ratio (*56*). 对于铝杂质，通过调节浸出液的pH值(57)，可以通过选择性沉淀去除大量铝杂质。For Al impurity, a significant amount can be removed through selective precipitation by adjusting the pH of the leach liquor (*57*). 钙和镁杂质通常不会与稀土元素共萃取，其公差上限为1500 ppm(58)，远高于我们浸出液中的含量(图S18至20)。Ca and Mg impurities usually do not co-extract with REE with the upper tolerance limit being 1500 ppm (*58*), which is much higher than the contents in our leach liquor (fig. S18 to 20). 因此，钙和镁在稀土元素提取中不是特别有问题。Thus, Ca and Mg are not particularly problematic in REE extraction. 对于铜和锌，在阳离子溶剂萃取或离子交换过程中，它们通常不会与稀土元素共萃取(58，59)。For Cu and Zn, they do not usually co-extract with REE during cation solvent extraction or ion exchange (*58*, *59*).

溶剂萃取分离稀土元素的探讨。
Discussion on the REE separation by solvent extraction.

目前，溶剂萃取是最合适的稀土分离商业技术。Nowadays, solvent extraction is the most appropriate commercial technology for REE separation. 分离通常由一次分离和二次分离完成。The separation is generally done by primary separation and secondary separation. 对于一次分离，由于高分配系数，D2EHPA通常用于从稀溶液中浓缩稀土元素。For the primary separation, D2EHPA is usually used to concentrate the REE from dilute solutions because of the high distribution coefficients. 随后，使用阳离子交换剂、溶剂化萃取剂和阴离子交换剂分离单个稀土元素。Subsequently, cation exchangers, solvation extractants, and anion exchangers are used to separate individual REE. 可以组装多达数百级的混合器和沉淀器，以实现必要的稀土元素分离和纯度，这已经是许多商业稀土元素提取厂的常规方案(51)。Up to hundreds of stages of mixer and settler may be assembled to achieve the necessary separation and purity of REE, which have already been the routine scheme in many commercial REE extraction plants (*51*).

我们的含稀土元素的浸出液可以通过类似的程序获得单个稀土元素。Our REE-containing leachates could undergo similar procedures to get the individual REE. 此外，通过增加水相pH值(51)，可以促进用阳离子交换剂萃取稀土元素。Moreover, the extraction of REE with cation exchangers is promoted by increasing the aqueous phase pH (*51*). 在这里，我们实现了在相对较高的pH值(例如，CFA-F的pH值为2，CFA-C的pH值为1)下的高REE浸出能力，因此获得的浸出液已经具有较高的pH值。Here, we realized the high REE leachability at a relatively high pH (*e.g.*, pH 2 for CFA-F, and pH 1 for CFA-C), so the as-obtained leach liquors already have high pH. 这可以减少使用化学试剂中和渗滤液，并有利于随后的稀土元素分离。This could reduce the use of chemical agents to neutralize the leachate and be beneficial for the subsequent REE separation. 因此，可以利用现有分离技术处理通过FJH获得的REE提取物。Hence, existing separations technologies can be exploited to work with the REE extracts obtained through FJH. FJH获得的混合物通常比采矿产生的混合物更简单，这代表了回收方案的另一个主要优点。The mixtures obtained by FJH are often less cumbersome than those generated through the mining of ores, which represent another major benefit of the recycling scheme.

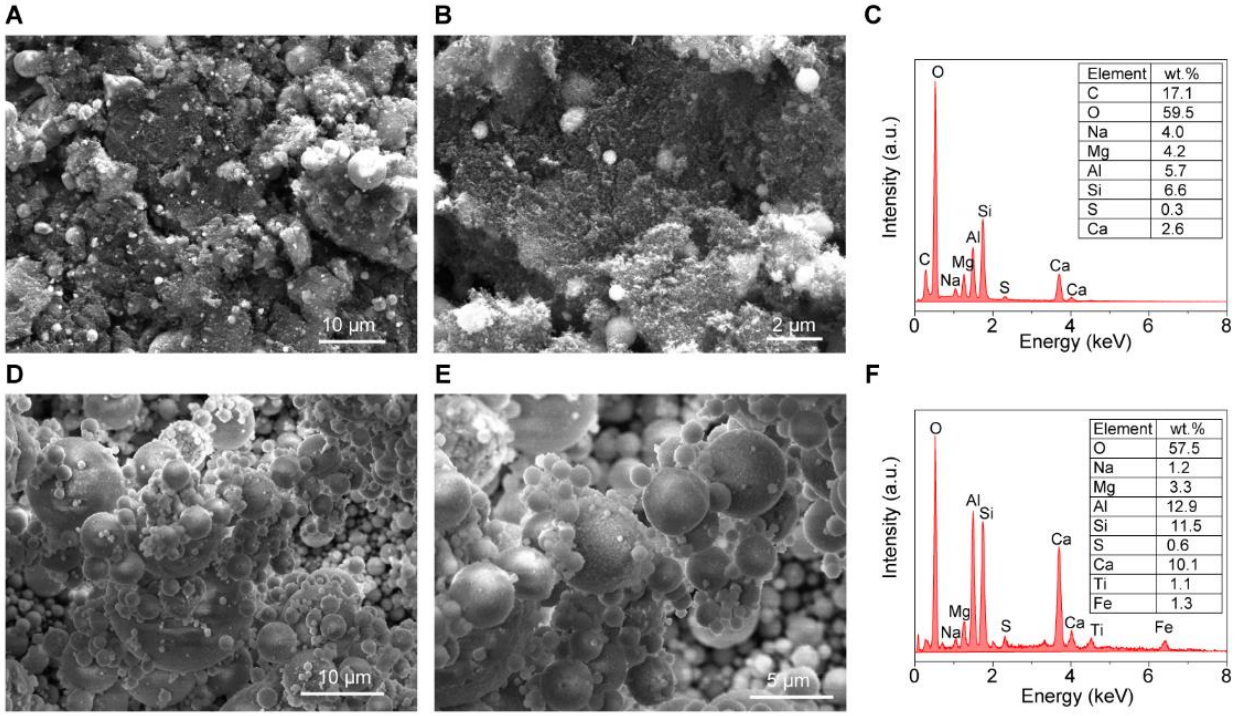

图S1。通过SEM和EDS对CFA的形态和成分进行表征。（A至B）CFA-F的SEM图像。（C）CFA-F的EDS光谱。插图，CFA-F中主要元素的重量百分比。（D到E）CFA-C的SEM图像。（F）CFA-C的EDS光谱。插图，CFA-C中主要元素的重量百分比。

Fig. S1. Morphology and composition characterization of CFA by SEM and EDS. (**A** to **B**) SEM images of CFA-F. (**C**) EDS spectrum of CFA-F. Inset, the weight percentage of major elements in CFA-F. (**D** to **E**) SEM images of CFA-C. (**F**) EDS spectrum of CFA-C. Inset, the weight percentage of major elements in CFA-C.

SEM图像显示，CFA-C由粒径为几到几十米的球形颗粒组成。

The SEM images show that the CFA-C is composed of spherical particles with size of a few to tens of μm. 相比之下，CFA-F的尺寸较小。In contrast, the size of CFA-F is smaller. CFA-F中的主要元素为C、O、Na、Mg、Al、Si、S和Ca。The major elements in CFA-F are C, O, Na, Mg, Al, Si, S, and Ca. CFA-C中的主要元素为O、Na、Mg、Al、Si、S、Ca、Ti和Fe。The major elements in CFA-C are O, Na, Mg, Al, Si, S, Ca, Ti, and Fe. CFA-F的C含量较高，而CFA-C的C含量可以忽略不计。The CFA-F has a high content of C while CFA-C has negligible C content. 相反，CFA-C中的钙含量显著高于CFA-F。In contrast, the Ca content in CFA-C is significantly higher than that in CFA-F. 以前的报告表明，钙含量越高，REE(4)的酸萃取性越高。Previous report showed that a higher content of Ca contributes to the higher acid extractability of REE (*4*).

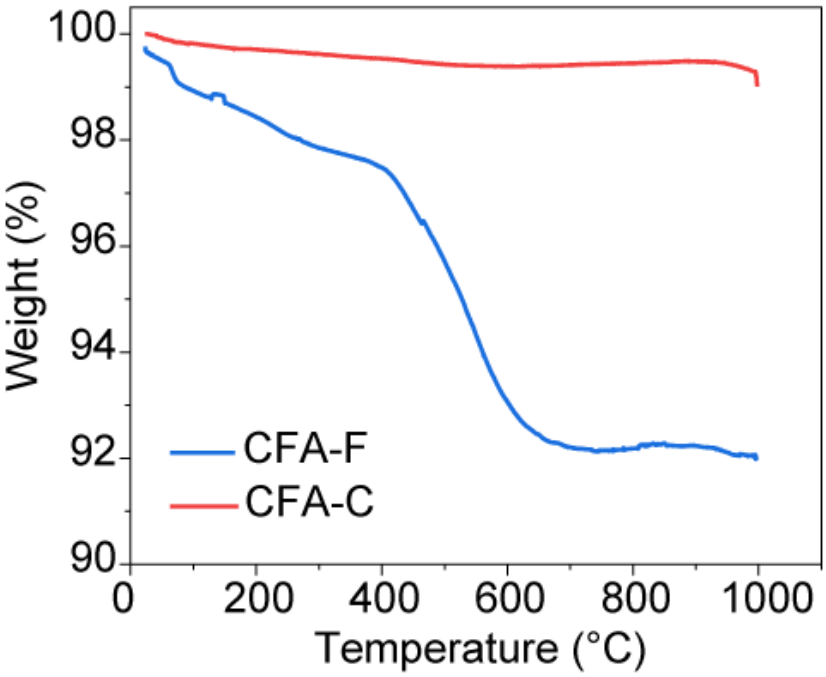

图S2。CFA在加热速率为10 ° C min-1的空气中的TGA曲线。

Fig. S2. TGA curve of CFA in air with a heating rate of 10 °C min^{-1}.

CFA-C的热重分析曲线显示，当温度上升到约700 ° C时，重量损失约为8 wt%。

The TGA curve of CFA-C shows an obvious weight loss of ~8 wt% when the temperature rises to ~700 °C. This is probably caused by the combustion of C, since there is a high C content in CFA-F according to the EDS analysis (fig. S1). In contrast, the CFA-F only shows a minor weight loss up to 1000 °C. In CFA, the major components are metal oxides, such as CaO, Fe_2O_3, and SiO_2, which are stable in air up to 1000 °C.

这可能是由C燃烧引起的，因为根据EDS分析(图S1)，CFA-F中的C含量较高。

相比之下，CFA-F在高达1000 ° C时仅显示轻微的重量损失。

在CFA中，主要成分是金属氧化物，如CaO、Fe2O3和SiO2，它们在高达1000 ° C的空气中稳定。

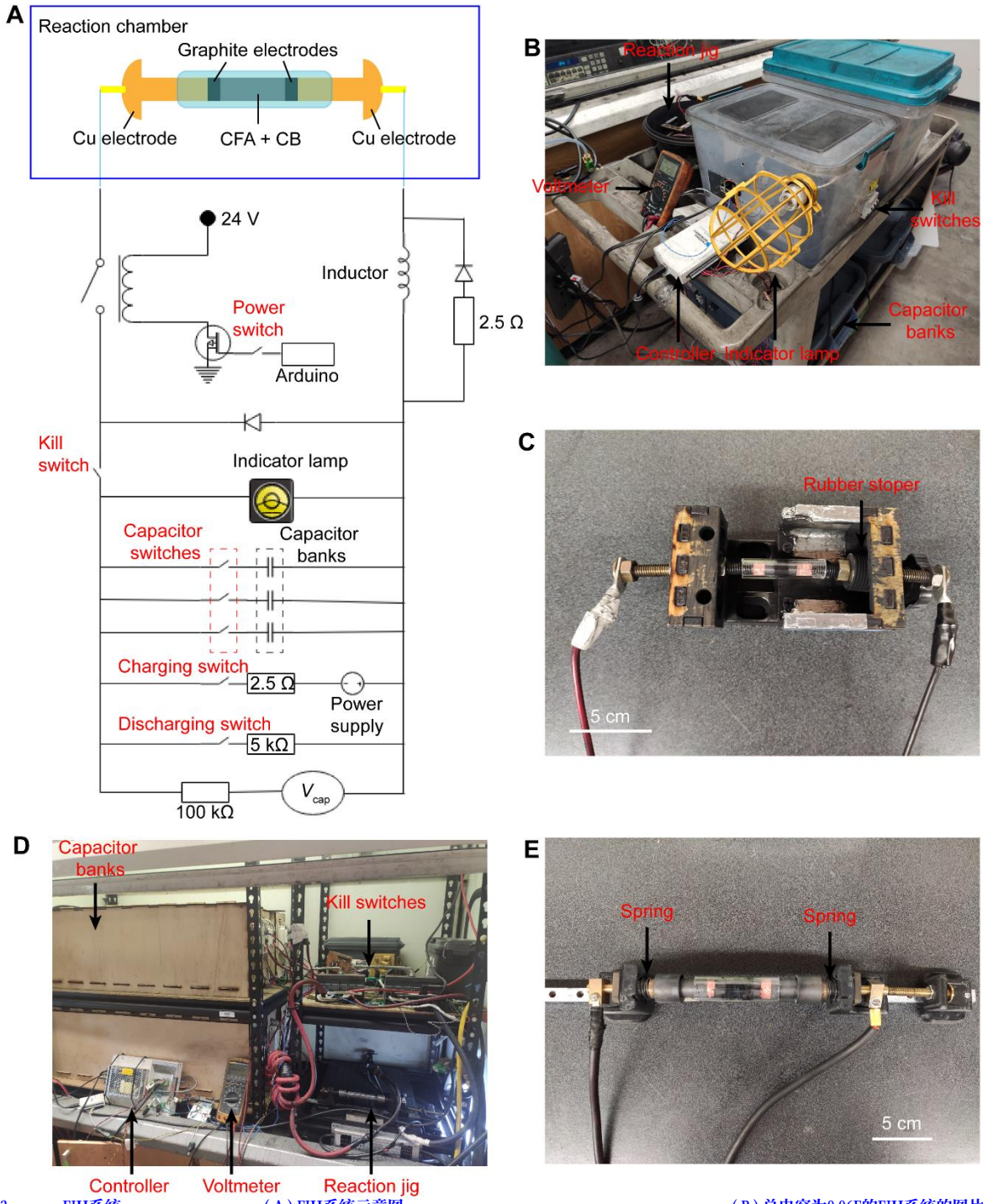

图S3。FJH系统。（A）FJH系统示意图。（B）总电容为0.06F的FJH系统的图片。（C）较小的FJH夹具连接样品和FJH系统，用于200 mg合成。（D）图为总电容为0.624F的较大FJH系统。（E）较大的FJH夹具用于连接样品和FJH系统进行2-g合成。在FJH过程中，（C）中的橡胶塞和（E）中的弹簧为样品提供逐渐压缩。

Fig. S3. The FJH system. (**A**) Schematic diagram of the FJH system. (**B**) The picture of the FJH system with the total capacitance of 0.06 F. (**C**) The smaller FJH jigs to connect the sample and the FJH system for 200-mg synthesis. (**D**) The picture of the larger FJH system with total capacitance of 0.624 F. (**E**) The larger FJH jigs to connect the sample and the FJH system for 2-g synthesis. The rubber stopper in (C) and the springs in (E) provide gradual compression to the sample during FJH.

电气部件：

Electrical components:

有关FJH系统中使用的电气部件的详细信息，请参阅我们之前的出版物(24)。

The details of the electrical components used in the FJH system could be found in our previous publication (*24*). 我们也在这里列出了其中的主要部分。We also listed major of them here.

1、电容器：铝电解电容器(Mouser#80-PEH200YX460BQU2，450 V，6 mF)。

1. Capacitors: Aluminum electrolytic capacitors (Mouser #80-PEH200YX460BQU2, 450 V, 6 mF). 对于较小的FJH系统，电容器组由10个这样的电容器组成，总电容为0.06F。For the smaller FJH system, the capacitor bank is composed of 10 such capacitors with the total capacitance of 0.06 F. 该电容器组适用于批量为0.5g的反应。This capacitor bank is suitable for the reaction with batch size ≤ 0.5 g. 对于较大的FJH系统，电容器组由104个此类电容器组成，总电容为0.624F。For the larger FJH system, the capacitor bank is composed of 104 such capacitors with the total capacitance of 0.624 F. 该电容器组适用于批量达10g的反应。This capacitor bank is suitable for the reaction with batch size up to 10 g.

2、机械继电器：900 V，500 A(TE Connectivity LEV200A5ANA)3、电源：LED电源299.6 W 214

2. Mechanical relay: 900 V, 500 A (TE Connectivity LEV200A5ANA)

428 V 700 mA(鼠标#709-HLG320H-C700B)。

3. Power supply: LED Power Supplies 299.6 W 214–428 V 700 mA (Mouser #709-HLG320H-C700B).

4 Vcap：万用表福禄克189

4. V_{cap}: Multimeter Fluke 189

充电和放电开关：400 V，6 A断路器(ABB S 282 K 6 A)

5. Charging and discharging switches: 400 V, 6 A breaker (ABB S 282 K 6 A)

6、电容器开关：277 V，10 A断路器(ABB S201P-C10)

6. Capacitor switches: 277 V, 10 A breaker (ABB S201P-C10)

7 Kill开关：440 V，630 A断路器(AAB S283 UC Z 63A)

7. Kill switch: 440 V, 630 A breaker (AAB S283 UC Z 63A)

8、电感器：24 mH(鼠标#553-C-80U)

8. Inductor: 24 mH (Mouser #553-C-80U)

控制器：Arduino Uno，带LCD显示屏

9. Controller: Arduino Uno with LCD display

10 电源：LED电源299.6 W 214-428 V 700 mA(鼠标器#709-HLG320H-C700B)

10. Power supply: LED Power Supplies 299.6 W 214-428 V 700 mA (Mouser #709-HLG320H-C700B)

安全指南：

Safety guidelines:

1、封闭或小心绝缘电线连接。

1. Enclose or carefully insulate the wire connections.

所有连接和导线必须适用于高电压和高电流。

2. All connections and wires must be suitable for high voltages and currents.

3、用户应遵守一只手规则：在系统上工作时只使用一只手，另一只手不得接触任何接地表面。

3. Users should obey the one hand rule: use only one hand when working on the system, with the other hand not touching any grounded surface.

4、请记住，系统可以在毫秒内放电数千焦耳，这可能导致继电器等部件爆炸。

4. Keep in mind that the system can discharge thousands of Joules in milliseconds, which could cause components such as relays to explode.

5、始终保持高压测试电压表可用。

5. Keep a voltmeter with high voltages test available at all times. 在电容器组上工作时，始终检查每个电容器组上的电压。When working on the capacitor banks, always check the voltage on each.

6、使用仪器时，戴上厚厚的橡胶手套，一直戴到肘部，以防触电。

6. Wear thick rubber gloves that extending to the elbows when using the apparatus to protect from electrocution.

系统的可靠性和鲁棒性应由经验丰富的电气技术人员确认。

7. The reliability and robustness of the system should be confirmed by an experienced electrical technician.

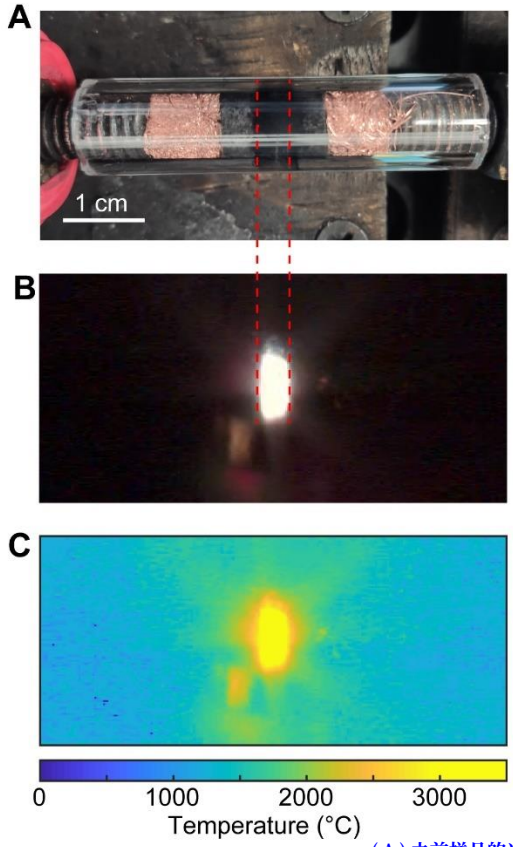

图S4。FJH期间样品的温度图。

Fig. S4. Temperature map of the sample during FJH. (A) 之前样品的光学图像 Optical image of the sample before FJH. (B) FJH期间样品的光学图像。 Optical image of the sample during FJH. (C) FJH期间样品的温度图。 Temperature map of the sample during FJH. 样品两侧的深色区域是石墨电极。 The dark regions on each side of the sample are graphite electrodes.

根据Stefan-Boltzmann定律，黑体辐射发射度(j)与黑体热力学温度(T)的四次方成正比，

According to the Stefan-Boltzmann law, the blackbody radiant emittance (j) is proportional to the fourth power of the blackbody's thermodynamic temperature (T),

$$j = \sigma T^4 \quad \text{(S19)}$$

=4(S19)，其中为比例常数。

相反，可以根据样品的辐射强度来评估样品的温度。

where σ is a constant of proportionality. Inversely, the temperature of a sample could be evaluated based on its radiant intensity. 在实验上，我们首先使用超快相机在FJH过程中捕获了样品的光学图像(图S4B)。 Experimentally, we first captured the optical image of a sample during FJH process using an ultrafast camera (fig. S4B). 然后，将彩色图像转换为灰度图像，并使用MATLAB将其进一步转换为强度矩阵。 Then, the color image was converted to a grayscale image, which was further converted to an intensity matrix using MATLAB. 根据红外温度计测量获得样品的最高温度(Tmax~2970°C)(图2C)，其对应于强度矩阵中的最大值(Imax)。 The highest temperature (T_{max} ~ 2970 °C) of the sample was obtained according to the IR thermometer measurement (Fig. 2C), which corresponds to the largest value (I_{max}) in the intensity matrix. 因此，可以基于斯特凡-玻尔兹曼定律，使用强度矩阵中的强度值(I)计算图像每个像素的温度(T)， Hence, the temperature (T) of each pixel of the image could be calculated using the intensity value (I) in the intensity matrix, based on the Stefan-Boltzmann law,

$$\frac{I}{I_{max}^{最大值}} = \left(\frac{T}{T_{max}^{最大值}}\right)^4 \quad \text{(S20)}$$

绘制了样品内的温度分布图(图S4C)。 The temperature distribution within the sample was plotted (fig. S4C). 发现整个样品的温度非常均匀，没有明显的梯度。 It is found that the temperature is very uniform throughout the entire sample without obvious gradient. 整个样品可以达到约3000°C的高温，表明FJH工艺具有均匀加热能力。 The whole sample could achieve a high temperature of ~3000 °C, demonstrating that the FJH process has a homogenous heating capability.

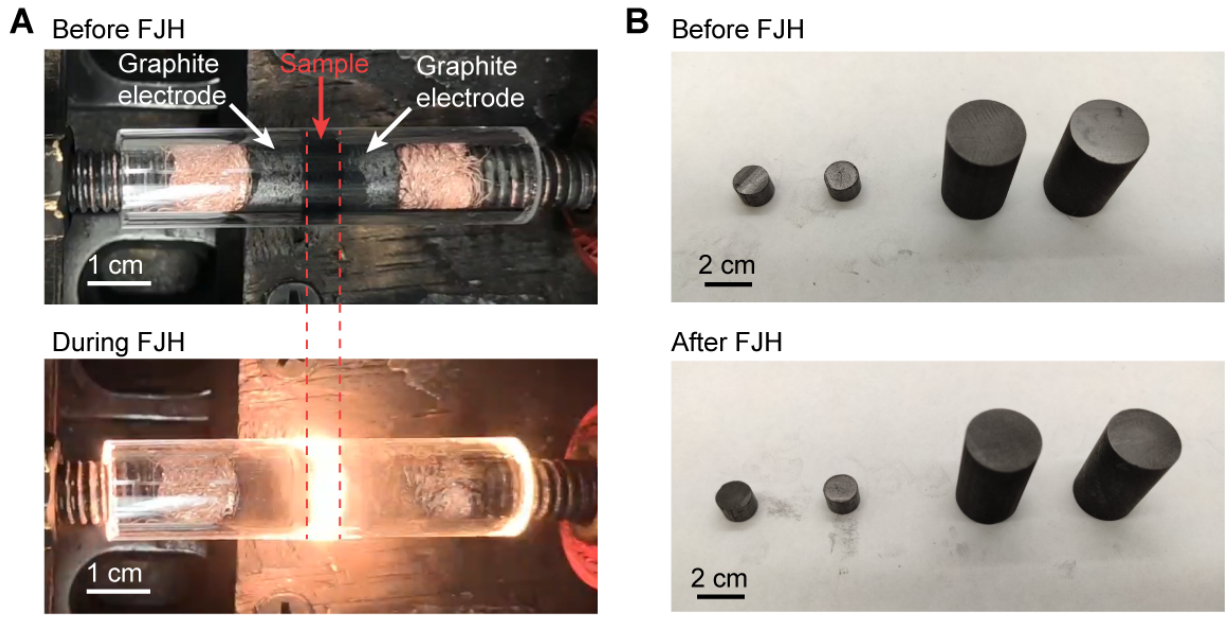

图S5。FJH系统的耐久性。（A）FJH之前（顶部）和期间（底部）样品的光学图像。（B）石墨电极在FJH之前（顶部）和之后（底部）的光学图像。

Fig. S5. Durability of the FJH system. (**A**) Optical images of the sample before (top) and during (bottom) the FJH. (**B**) Optical images of the graphite electrodes before (top) and after (bottom) the FJH.

FJH装置具有良好的耐久性。FJH工艺可以实现高温（~3000 °C），但高温区域仅限于样品。根据焦耳加热方程，

The FJH setup has good durability. A high temperature (~3000 °C) could be achieved by the FJH process, but the high-temperature region is only limited to the sample. According to the Joule heating equation,

Q=2（S21），其中I是通过样品的电流，R是样品的电阻，t是放电时间，电热与电阻成比例。

$$Q = I^2 Rt \quad (S21)$$

where I is the current passing through the sample, R is the resistance of the sample, and t is the discharging time, the electrical heat is proportional to the resistance. 石墨电极的电阻比样品小得多。The graphite electrodes have much smaller resistance than the sample. 因此，放电过程产生的热量施加在样品上。Hence, the heat generated by the discharging process is imposed on the sample. 如图S5A所示，在FJH过程中，样品区域的强发光受到限制，而石墨电极和FJH系统的其他部分保持在相对较低的温度。As shown in fig. S5A, the strong light emission is limited on the sample region during the FJH process, while the graphite electrodes and other parts of the FJH system remain at relatively low temperatures. 石墨电极具有良好的热稳定性。Graphite electrode has good thermal stability. 此外，FJH时间很短，温度为3000 °C，时间为几十毫秒（图2C）。In addition, the FJH time is very short, with the 3000 °C temperature in tens of milliseconds (Fig. 2C). 在FJH工艺后，石墨棒没有显示出明显的变化（图S5B），电阻保持不变。The graphite rods show no obvious change after the FJH process (fig. S5B), and the resistance remains the same. 因此，FJH工艺不会损坏电极。Hence, the FJH process will not damage the electrodes. FJH系统的其他部分是远离高温样品的商用电气元件，如导线和电容器。Other parts of the FJH system are commercial electrical components such as conductive wires and capacitors, which are far away from the high-temperature sample. 在我们的实验中，相同的FJH装置被使用了数百次，没有降解。The same FJH setup was used for hundreds of times for our experiments without degradation. 因此，我们得出结论，FJH系统具有很好的耐久性。Hence, we concluded that the FJH system has very good durability.

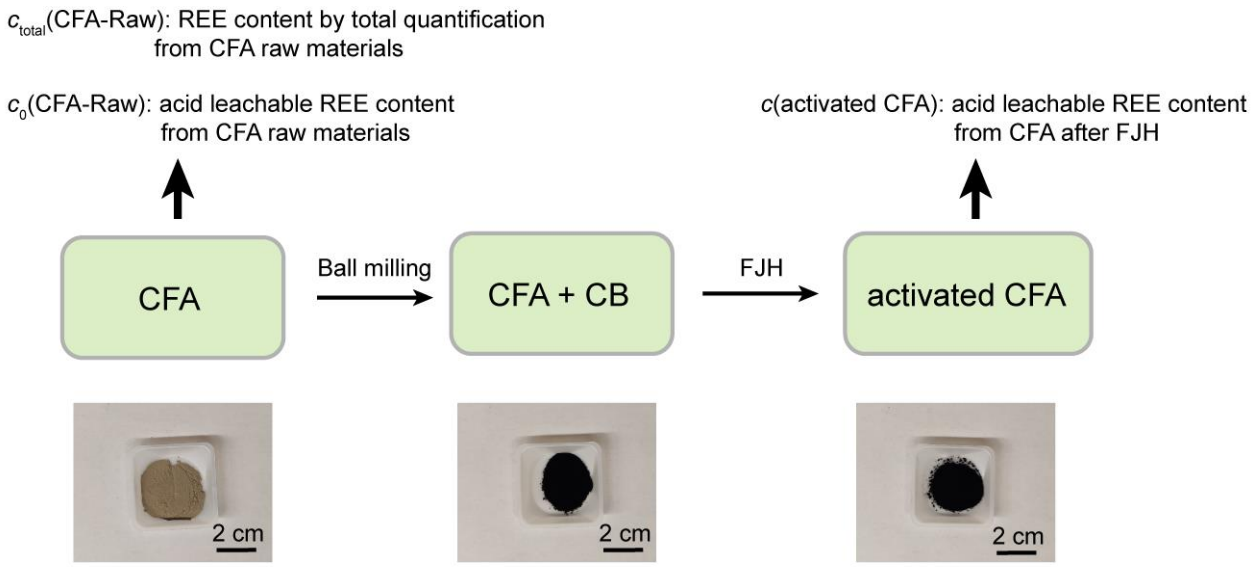

图S6。通过电热活化从二次废物中回收稀土元素的流程图。

Fig. S6. Flow chart of REE recovery from secondary wastes by electrothermal activation.

使用HF-HNO3消解法通过全消解测量CFA原料ctotal（CFA raw）中的总稀土含量（详见材料和方法）。

The total REE content in CFA raw materials, c_{total}(CFA-Raw), was measured by total digestion using a HF-HNO_3 digestion method (see details in Materials and Methods). 通过对CFA原料进行HCl或HNO3浸出，测定了CFA原料c0（CFA原料）中可酸浸出的稀土元素含量。The acid-leachable REE contents in CFA raw materials, c_0(CFA-Raw), were measured by HCl or HNO_3 leaching of the CFA raw materials. 将CFA原料和炭黑混合并进行FJH活化过程。The CFA raw materials and carbon black were mixed and underwent the FJH activation process. 获得的固体称为活化CFA。The obtained solid is termed as activated CFA. 采用与活化CFA相同的酸浸程序测量活化CFA中可酸浸的稀土元素含量c（活化CFA）。The acid-leachable REE contents in activated CFA, c(activated CFA), were measured by the same acid leaching procedure of the activated CFA. 然后，通过酸浸CFA原料和活化CFA计算稀土回收率（补充文本1）。Then, the REE recovery yield by acid leaching of the CFA raw materials, and the activated CFA were calculated (Supplementary Text 1).

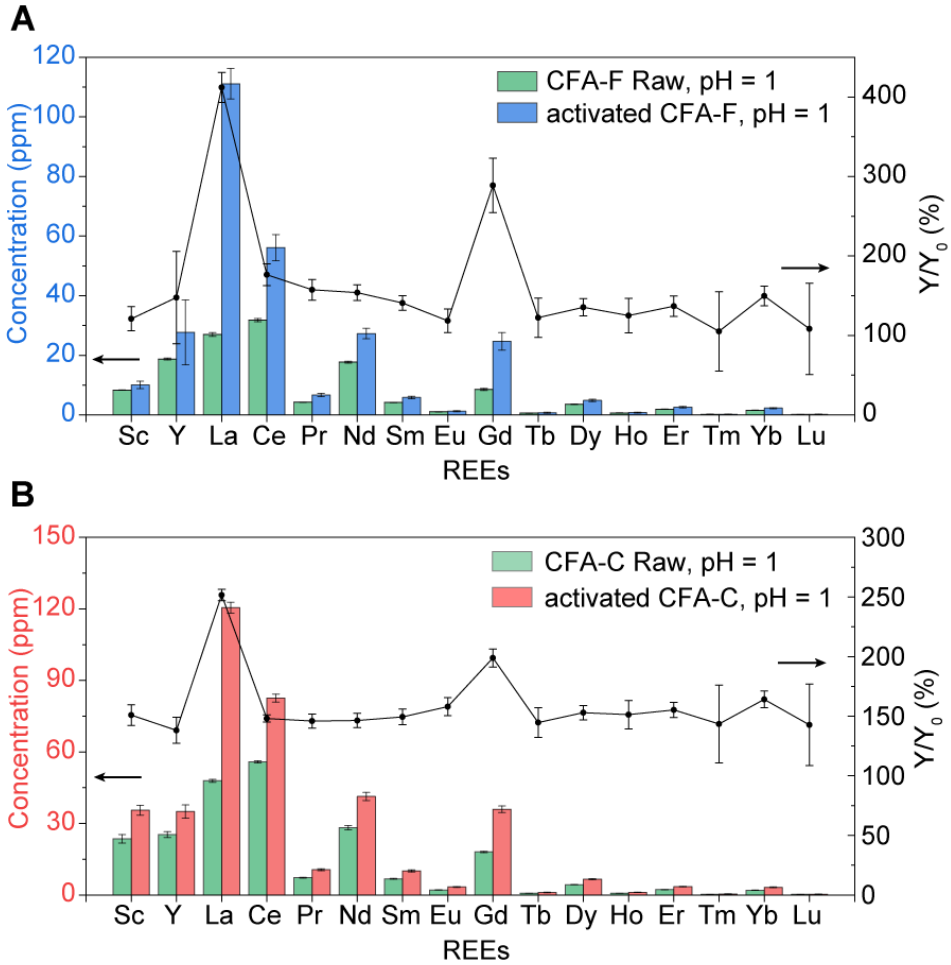

图S7。使用0.1 M HCl从CFA中浸出稀土的能力。（A）酸浸出稀土元素含量（0.1 M HCl，85 ° C）和活化的CFA-F，并提高回收率。（B）CFA-C原料和活化的CFA-C中可酸浸的稀土元素含量（0.1 M HCl，85 ° C），并提高回收率。Y0表示0.1 M HCl浸出CFA原料的稀土回收率，Y表示0.1 M HCl浸出活化CFA的稀土回收率。对于所有稀土元素，Y/Y0的平均值均大于100%，表明FJH工艺提高了回收率。A和B中的误差线表示标准偏差，其中N=3。

Fig. S7. REE leachability from CFA using 0.1 M HCl. (A) Acid-leachable REE contents (0.1 M HCl, 85 °C) from CFA-F raw materials and the activated CFA-F, and the increase of recovery yield. **(B)** Acid-leachable REE contents (0.1 M HCl, 85 °C) from CFA-C raw materials and the activated CFA-C, and the increase of recovery yield. Y_0 represents the REE recovery yield by 0.1 M HCl leaching the CFA raw materials, and Y represents the REE recovery yield by 0.1 M HCl leaching the activated CFA. For all the REE, the average values of Y/Y_0 were >100%, indicating that the FJH process increased the recovery yields. The error bars in A and B represent the standard derivation where N = 3.

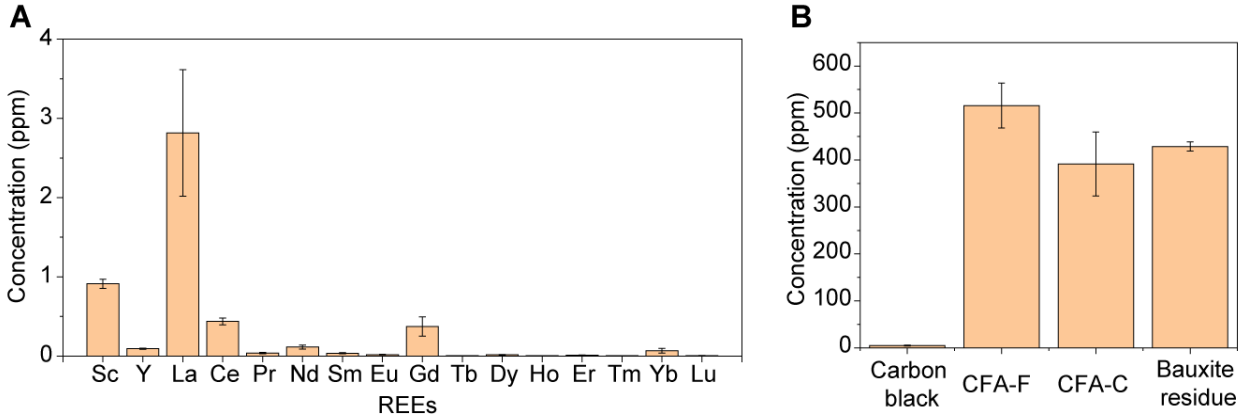

图S8。炭黑中稀土元素含量。（A）炭黑中单个稀土元素含量。（B）炭黑、CFA-F、CFA-C和铝土矿残渣（BR）中的总稀土含量。（A）和（B）中的所有误差线表示标准偏差，其中N=3。

Fig. S8. REE contents in carbon black. (A) Individual REE content in carbon black. **(B)** Total REE content in carbon black, CFA-F, CFA-C, and bauxite residue (BR). All error bars in (A) and (B) represent the standard deviation where N = 3.

炭黑中稀土元素含量较低，约为CFA-F中稀土元素含量的1.0%，CFA-C中稀土元素含量的1.3%，BR中稀土元素含量的1.2%。因此，炭黑添加剂不会在我们的测量中产生显著误差。

The REE contents in carbon black are low, ~1.0% of the REE contents in CFA-F, ~1.3% of the REE contents in CFA-C, and ~1.2% of the REE contents in BR. Hence, the carbon black additive will not induce significant error in our measurement.

此外，炭黑不是作为导电添加剂的唯一选择。在实际应用中，如果需要，炭黑可以用无烟煤替代，也可以用任何其他廉价的中等导电碳源替代。在我们的案例中，我们仅使用炭黑，因为其稀土元素含量较低，以排除导电添加剂引起的误差源。

In addition, carbon black is not the only choice as the conductive additive. In practical applications, the carbon black could be substituted with anthracite coal if desired, of any other inexpensive sources of mildly conductive carbon. In our cases, we used carbon black only since its REE content is low to exclude the error source induced by the conductive additive.

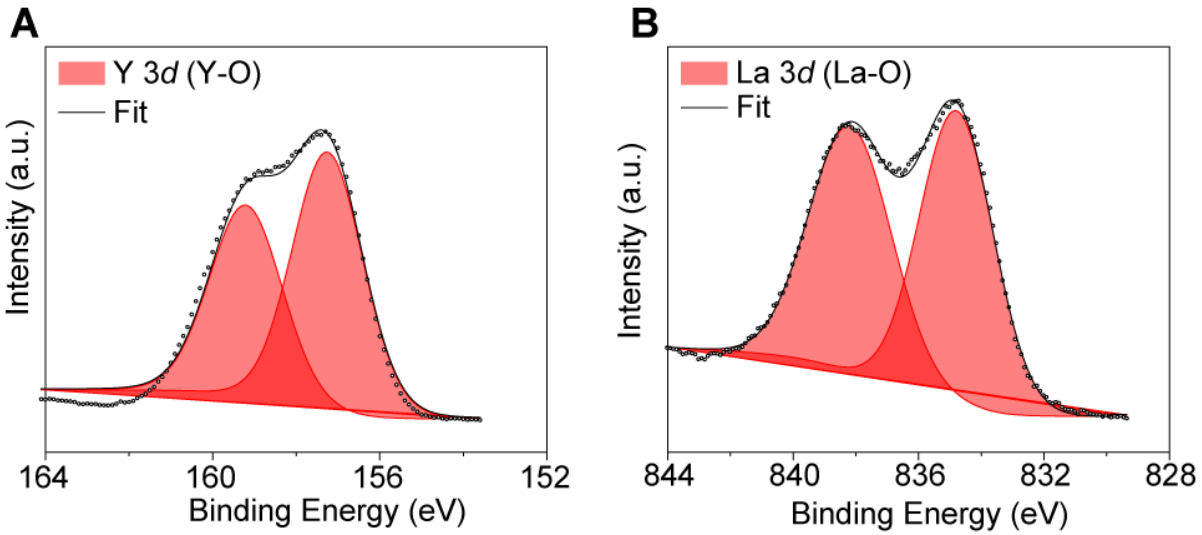

图S9。稀土氧化物的XPS表征。（A）Y2O3前驱体中Y的XPS精细光谱。

Fig. S9. XPS characterization of REE oxides. (**A**) XPS fine spectrum of Y in Y_2O_3 precursor. （B）La2O3前驱体中La的XPS精细光谱。(**B**) XPS fine spectrum of La in La_2O_3 precursor.

La2O3、FJH后La2O3、Y2O3和FJH后Y2O3的详细峰值拟合如表S4所示。

The detailed peak fittings for La_2O_3, La_2O_3 after FJH, Y_2O_3, and Y_2O_3 after FJH are shown in table S4. The Y 3*d* was split into $3d_{5/2}$ and $3d_{3/2}$. Y-3d分为3d5/2和3d3/2。在Y2O3中，3d5/2和3d3/2的峰值位置分别为157.4 eV和159.4 eV，与文献报道(35，36)吻合良好。In Y_2O_3, the peak positions for $3d_{5/2}$ and $3d_{3/2}$ are 157.4 eV and 159.4 eV, respectively, matching well with the literature reports (*35*, *36*). FJH后，Y 3d由四个峰值拟合(图3E)。After FJH, the Y 3*d* were fitted by four peaks (Fig. 3E). 157.5ev和159.6ev处的峰值分别分配给Y2O3中Y的3d5/2和3d3/2。The peaks at 157.5 eV and 159.6 eV are assigned to $3d_{5/2}$ and $3d_{3/2}$ of Y in Y_2O_3, respectively. 156.4 eV和158.5 eV处的峰值分配给Y金属中Y的3d5/2和3d3/2分别与文献报道(36)吻合良好。The peaks at 156.4 eV and 158.5 eV are assigned to $3d_{5/2}$ and $3d_{3/2}$ of Y in Y metal, respectively, matching well with the literature report (*36*). XPS分析表明，在FJH过程中，Y2O3被还原为Y金属，而Y2O3的小比例可能来自表面氧化。The XPS analysis showed that the Y_2O_3 is reduced to Y metal during the FJH process, while the small ratio of Y_2O_3 might be from the surface oxidation.

对于La2O3，834.8 eV和838.2 eV处的峰值对应于3d5/2及其卫星峰值(38，60)。For La_2O_3, the peaks at 834.8 eV and 838.2 eV correspond to $3d_{5/2}$ and its satellite peak (*38*, *60*). FJH后，除了834.8 eV和838.1 eV时La2O3的峰值(La 3d5/2及其卫星峰)外，峰值拟合(图3F，表S4)显示了836.0 eV和838.1 eV时的主要成分After FJH, in addition to the peaks from La_2O_3 at 834.8 eV and 838.1 eV (La 3*d*$_{5/2}$ and its satellite peak), the peak fitting (Fig. 3F, table S4) shows major components at 836.0 eV and 839.6 eV，分配给La 3d5/2和La metal的jt卫星峰，与文献报告(37，61)吻合良好。839.6 eV, which are assigned to La 3*d*$_{5/2}$ and it satellite peak from La metal, matching well with literature reports (*37*, *61*). XPS分析表明，在FJH过程中，La2O3被还原为La，而较小比例的La2O3可能来自表面氧化。The XPS analysis showed that La_2O_3 were reduced to La during the FJH process, while the small ratio of La_2O_3 might be from the surface oxidation.

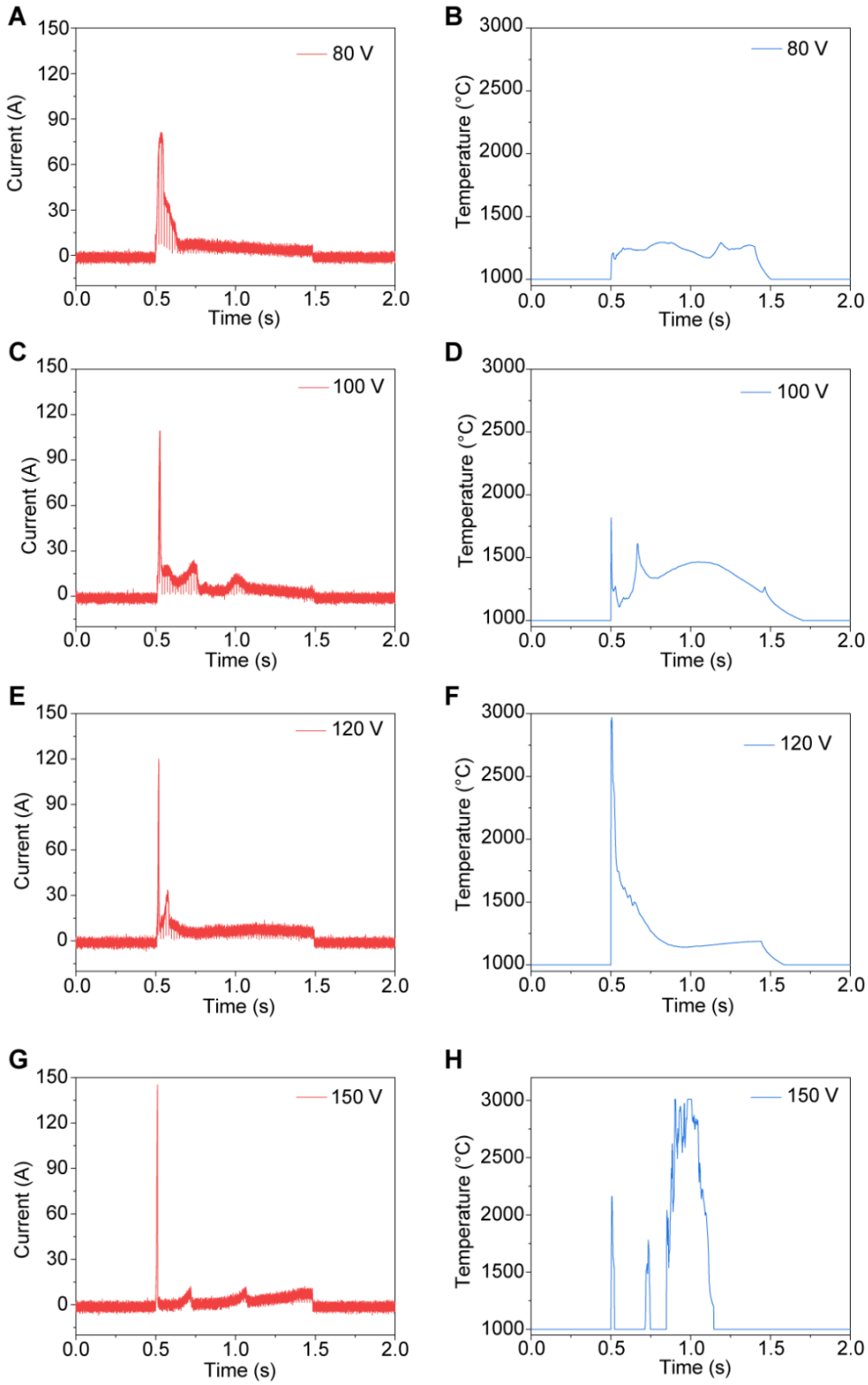

图S10。温度测量。电流曲线和实时温度曲线(A到B)80 V 1 s，(C到D)100 V 1 s，(E到F)120 V 1 s，和(G到H)150 V 1 s。

Fig. S10. Temperature measurement. Current curves and real-time temperature curves for (**A** to **B**) 80 V for 1 s, (**C** to **D**) 100 V for 1 s, (**E** to **F**) 120 V for 1 s, and (**G** to **H**) 150 V for 1 s.

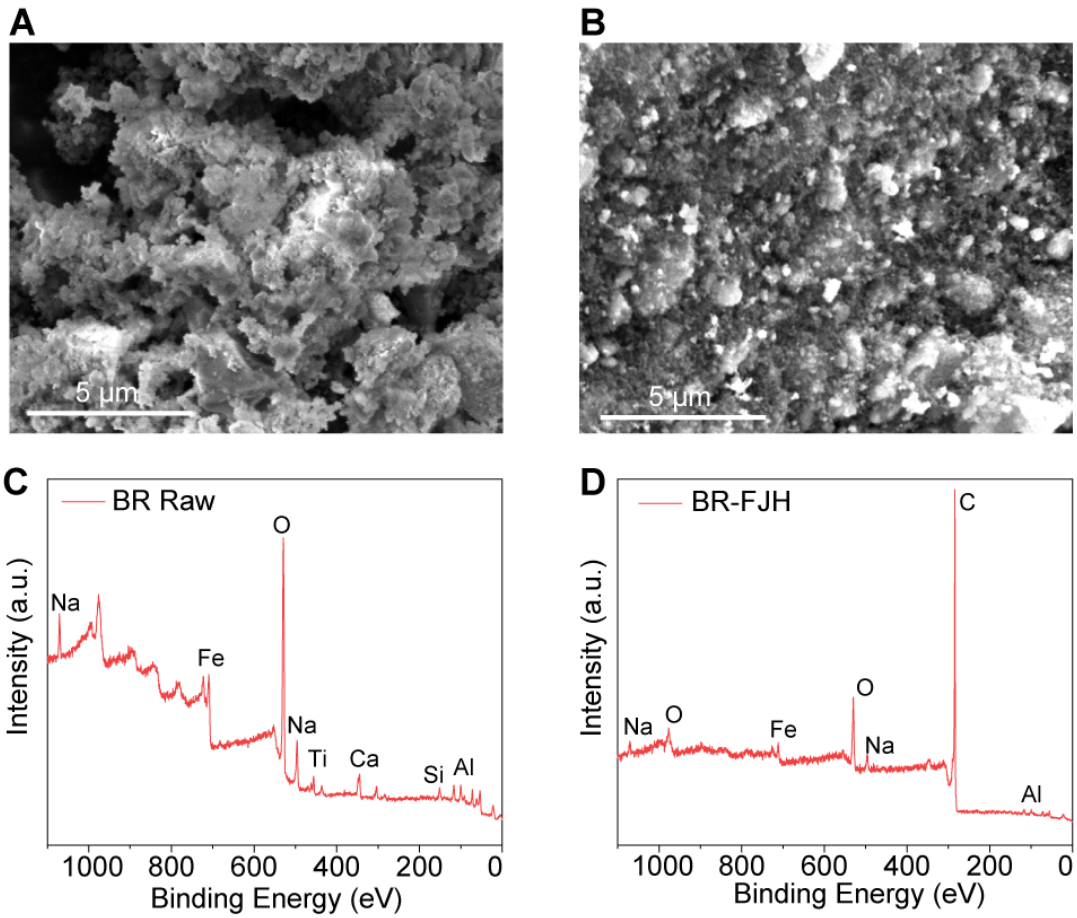

图S11。丁苯橡胶和丁苯橡胶经FJH后的表征。（A）BR原料的SEM图像。

Fig. S11. Characterization of BR and BR after FJH. (A) SEM image of BR raw materials. **(B)** FJH后BR的SEM图像。（C）BR原料的XPS光谱。（D）溴经FJH后的XPS光谱。

SEM image of BR after FJH. **(C)** XPS spectrum of BR raw materials. **(D)** XPS spectrum of BR after FJH.

经过FJH后，BR（图S11B）的粒径小于BR原料（图S11A），这将有助于酸浸。

After FJH, the particle size of the BR (fig. S11B) becomes smaller than the BR raw materials (fig. S11A), which would be helpful for the acid leaching. 根据XPS，经过FJH后，BR中的O含量显著降低，表明BR中的金属成分碳热还原。 According to the XPS, after FJH, the O content in BR is significantly reduced, demonstrating the carbothermic reduction of the metal components in BR. 这也有助于稀土元素的酸浸，原因与我们在正文中解释的从CFA中回收稀土元素的原因相同（图3）。 This would also contribute to the acid leaching of REE for the same reasons we have explained for the recovery of REE from CFA in the main text (Fig. 3).

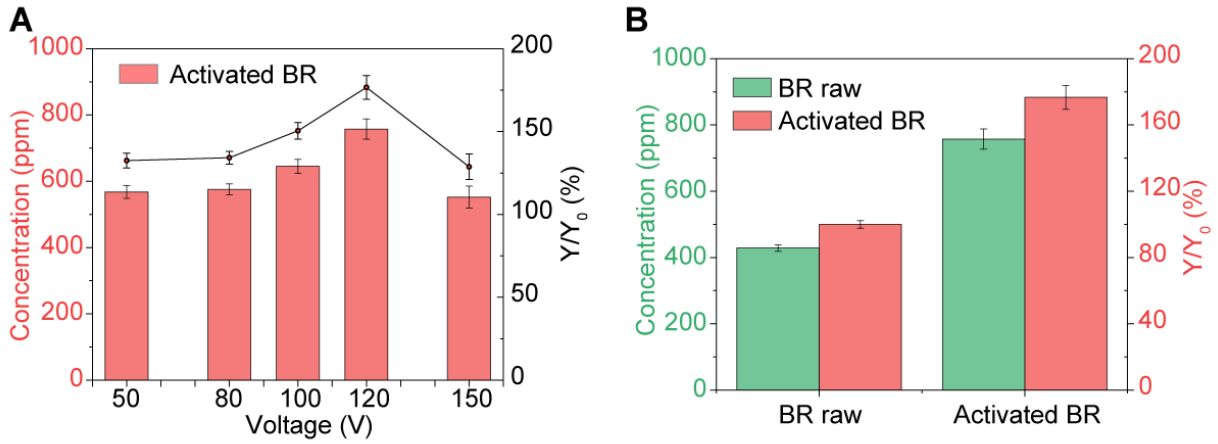

图S12。BR的FJH电压相关稀土元素回收率。（A）酸浸出物含量

Fig. S12. FJH voltage dependent REE recovery yield from BR. (A) Acid leachable content of total REE (0.5 M HNO_3) from BR, and the increase of REE yield varied with FJH voltages. **(B)** The acid leachable REE content (0.5 M HNO_3), and the increase of recovery yield at 120 V FJH. Y_0 represents the REE recovery yield by directly leaching the BR raw materials. *Y* represents the REE recovery yield by leaching the activated BR. The error bar in A and B denotes the standard deviation where N = 3.

BR中的总稀土元素(0.5 M HNO3)，稀土产率的增加随FJH电压的变化而变化。在120 V FJH下，可酸浸REE含量(0.5 M HNO3)和回收率的增加。Y0表示直接浸出BR原料的稀土回收率。Y表示通过浸出活化溴得到的稀土回收率。A和B中的误差条表示标准偏差，其中N=3。

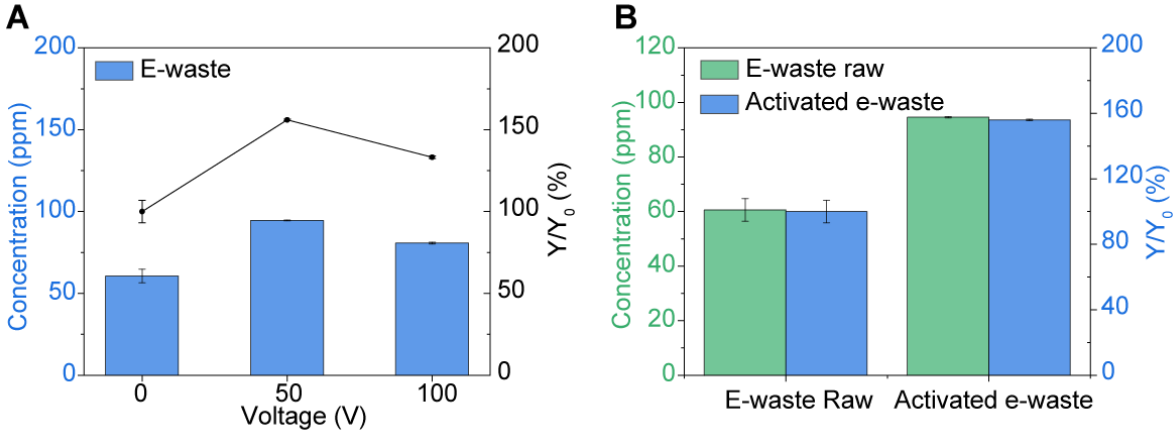

图S13。通过FJH活化提高电子垃圾中稀土元素的回收率。（A）酸性-

Fig. S13. Improving the REE recovery yield from e-waste by FJH activation. (A) Acid-leachable content of total REE (1 M HCl) from e-waste, and the increase of REE recovery yield varied with the FJH voltages. **(B)** The acid leachable content of total REE (1 M HCl), and the increase of REE recovery yield at 50 V FJH. Y_0 represents the REE recovery yield by directly leaching the e-waste raw materials. *Y* represents the REE recovery yield by leaching the activated e-waste. The error bars in A and B denote the standard deviation where N = 3.

电子垃圾中总稀土元素(1 M HCl)的可浸出含量以及稀土元素回收率的增加随FJH电压的变化而变化。（B）在50 V FJH下，总稀土元素(1 M HCl)的可酸浸含量和稀土回收率的增加。Y0表示直接浸出电子废物原料的稀土回收率。Y表示通过浸出活化电子废物获得的稀土元素回收率。A和B中的误差线表示标准偏差，其中N=3。

The optimized FJH voltage for recovering REE from e-waste is 50 V. Too high voltage, which leads to too high temperature, might result in the evaporative loss of REE. The acid leachable content of total REE from the activated e-waste is ~95 ppm, corresponding to ~156% of the leachable REE content from e-waste raw materials.

从电子垃圾中回收稀土元素的最佳FJH电压为50V。电压过高会导致温度过高，可能导致稀土元素的蒸发损失。活化电子废物中总稀土元素的可酸浸出含量约为95 ppm，相当于电子废物原料中可浸出稀土元素含量的156%。

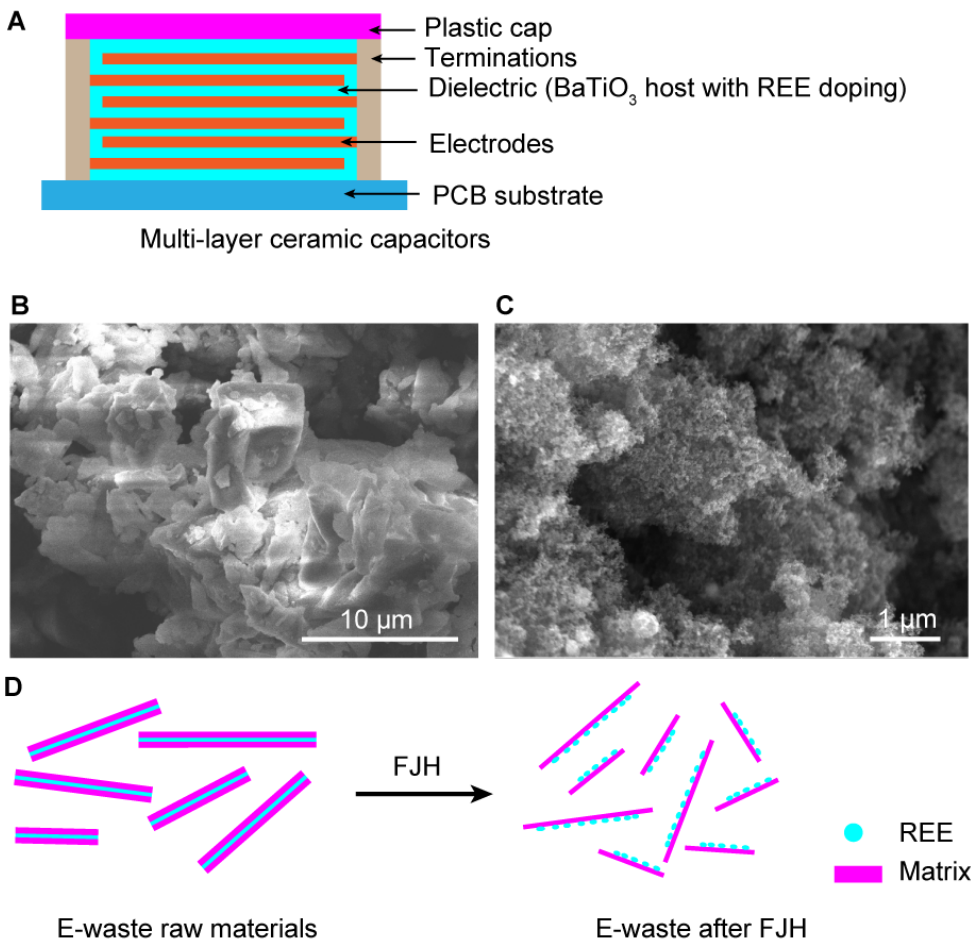

图S14。FJH活化提高电子垃圾中稀土回收率的机理。

Fig. S14. Mechanism of the improved REE recovery yield in e-waste by FJH activation. (**A**) 多层陶瓷电容器的结构方案。 (B)电子垃圾破碎后的SEM图像。 Structure scheme of the multi-layer ceramic capacitors. (**B**) SEM image of the e-waste after crushing. (C)电子垃圾经过FJH后的SEM图像。 (**C**) SEM image of the e-waste after FJH. (D)FJH过程中电子垃圾的形态变化方案。 (**D**) Scheme of the morphology change of the e-waste during the FJH process.

稀土元素广泛应用于现代电子产品中，如强磁体、陶瓷电容器等。 The REE are widely used in modern electronics as strong magnets, ceramic capacitors, *etc*. 大多数电子设备具有层压结构，例如多层陶瓷电容器(44)(图S14A)，REE被塑料和陶瓷的隔离层和保护层覆盖。 Most electronic devices have the laminated structures, *e.g.*, the multilayer ceramic capacitors (*44*) (fig. S14A), and the REE are covered by the separator and protection layer of plastics and ceramics. 层状结构通过防止稀土物种暴露于浸出剂而使稀土元素浸出变得困难。 The laminated structure makes it difficult for REE leaching by preventing the exposure of REE species to leachant. 即使在研磨后，电子垃圾的粒径也很大(图S14B)。 Even after grinding, the particle size of the e-waste is large (fig. S14B). 在FJH工艺后，层状结构被破坏(图S14C至D)，这提供了可酸浸的稀土元素。 After the FJH process, the laminated structures are broken (fig. S14C to D), which affords the acid leachable REE.

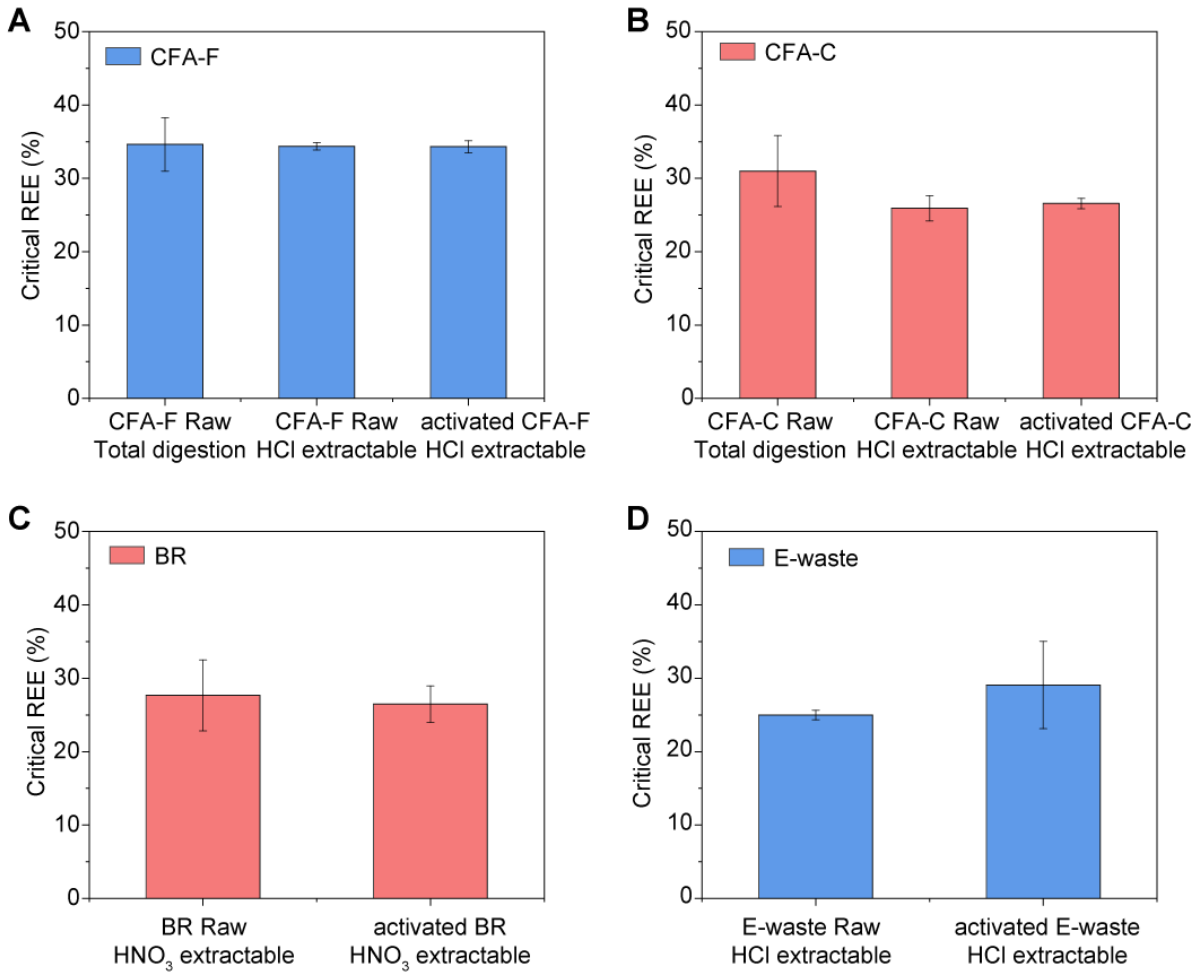

图S15。临界稀土元素在总稀土元素中的百分比。(A)CFA中临界稀土元素的百分比-

Fig. S15. The percentage of critical REE in total REE. (A) Percentage of critical REE in CFA-F, 包括总消化量、CFA-F原料中HCl(1M，85°C)可提取稀土含量和活化CFA-F中HCl可提取稀土含量。including the total digestion, HCl (1 M, 85 °C) extractable REE content in CFA-F Raw materials, and HCl extractable REE content in activated CFA-F. **(B)** Percentage of critical REE in (B)CFA-C中临界稀土元素的百分比，包括总消化、CFA-C原料中HCl(1M，85°C)可萃取稀土元素含量和活化CFA-C中HCl可萃取稀土元素含量。CFA-C, including the total digestion, HCl (1 M, 85 °C) extractable REE content in CFA-C Raw materials, and HCl extractable REE content in activated CFA-C. **(C)** Percentage of critical REE (C)BR中临界稀土元素的百分比、包括BR原料中HNO3(0.5M，RT)可萃取稀土元素含量，以及活化BR中HNO3可萃取稀土元素含量。in BR, including the HNO_3 (0.5 M, RT) extractable REE content in BR Raw materials, and HNO_3 extractable REE content in activated BR. **(D)** Percentage of critical REE in e-waste, including the (D)电子废物中关键稀土元素的百分比，包括电子废物原料中的HCl(1M，85°C)可提取稀土元素含量，以及活化电子废物中的HCl可提取稀土元素含量。HCl (1 M, 85 °C) extractable REE content in e-waste Raw materials, and HCl extractable REE content in activated e-waste. The critical REE include Y, Nd, Eu, Tb, and Dy. 关键稀土元素包括Y、Nd、Eu、Tb和Dy。All error bars in (A) to (D) denote standard deviation where N = 3. (A)至(D)中的所有误差线表示标准偏差，其中N=3。

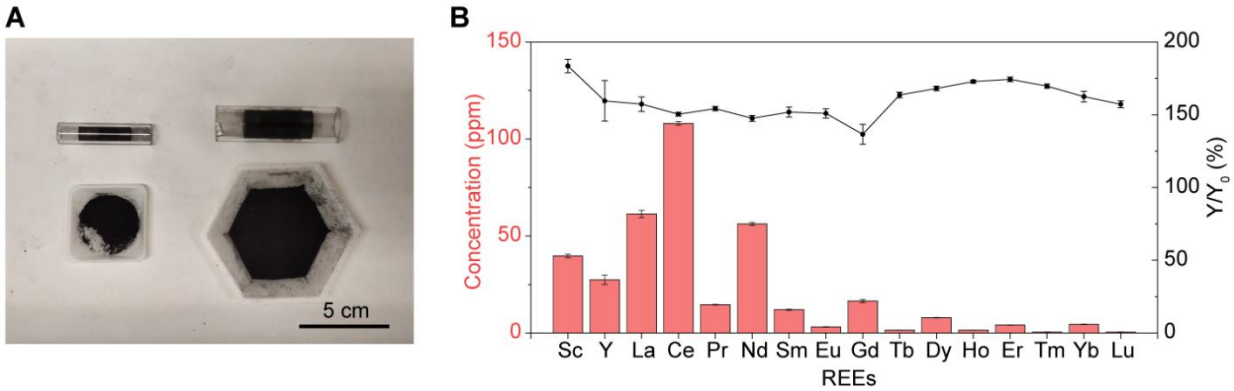

图S16。以CFA-C为例放大电热活化过程。

Fig. S16. Scaling up of the electrothermal activation process by using CFA-C as an example.

(A)质量为m0=200 mg、石英管直径为D0=8 mm(左)的小样品和质量为m1=2 g、管直径为D1=16 mm(右)的大样品的照片。(B)在质量为m1=2 g的活化CFA-C中，可酸浸出的稀土元素含量(1M HCl，85 °C)和回收率的增加。Y0表示直接浸出CFA-C原料的稀土回收率。Y表示通过浸出活化CFA-C获得的稀土回收率。(B)中的误差线表示标准偏差，其中N=3。

(**A**) Picture of the small sample with mass of m_0 = 200 mg and quartz tube diameter of D_0 = 8 mm (left), and larger sample with mass of m_1 = 2 g and tube diameter of D_1 = 16 mm (right). (**B**) Acid leachable REE contents (1 M HCl, 85 °C) in activated CFA-C with the mass of m_1 = 2 g, and the increase of recovery yield. Y_0 represents the REE recovery yield by directly leaching the CFA-C raw materials. Y represents the REE recovery yield by leaching the activated CFA-C. The error bars in (B) denote the standard deviation where N = 3.

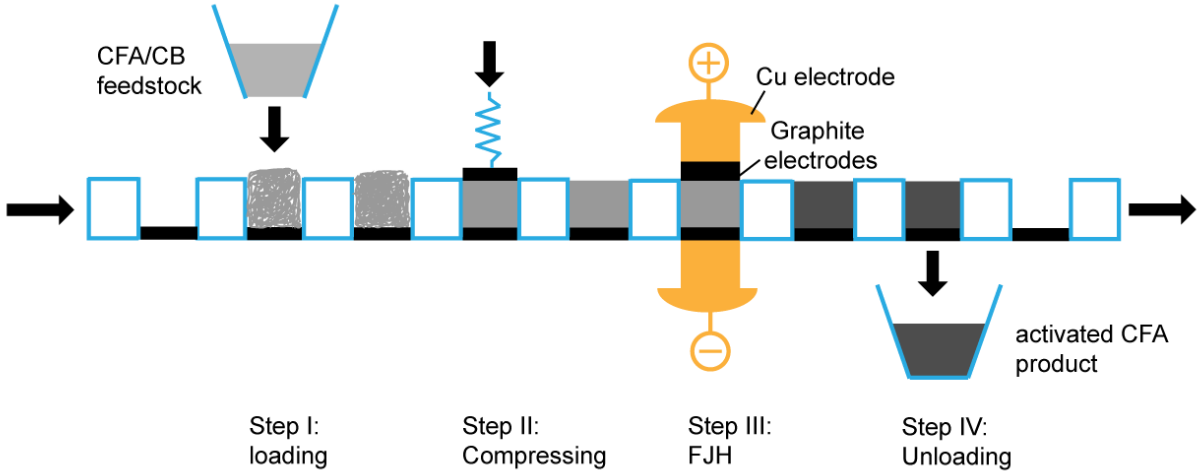

图S17。连续FJH反应器的概念样机设计。

Fig. S17. Conceptual prototype design of the continuous FJH reactor.

连续生产过程包括四个步骤。首先，将CFA/CB原料的混合物装载到传送带上的腔室中。其次，将样品压缩至特定电阻。第三，样品进行FJH反应。最后，收集活化的CFA产物。

The continuous production process consists of four steps. First, the mixture of CFA/CB feedstock is loaded onto the chamber on the conveyor belt. Secondly, the sample is compressed to a specific resistance. Thirdly, the sample undergoes the FJH reaction. Lastly, the activated CFA product is collected.

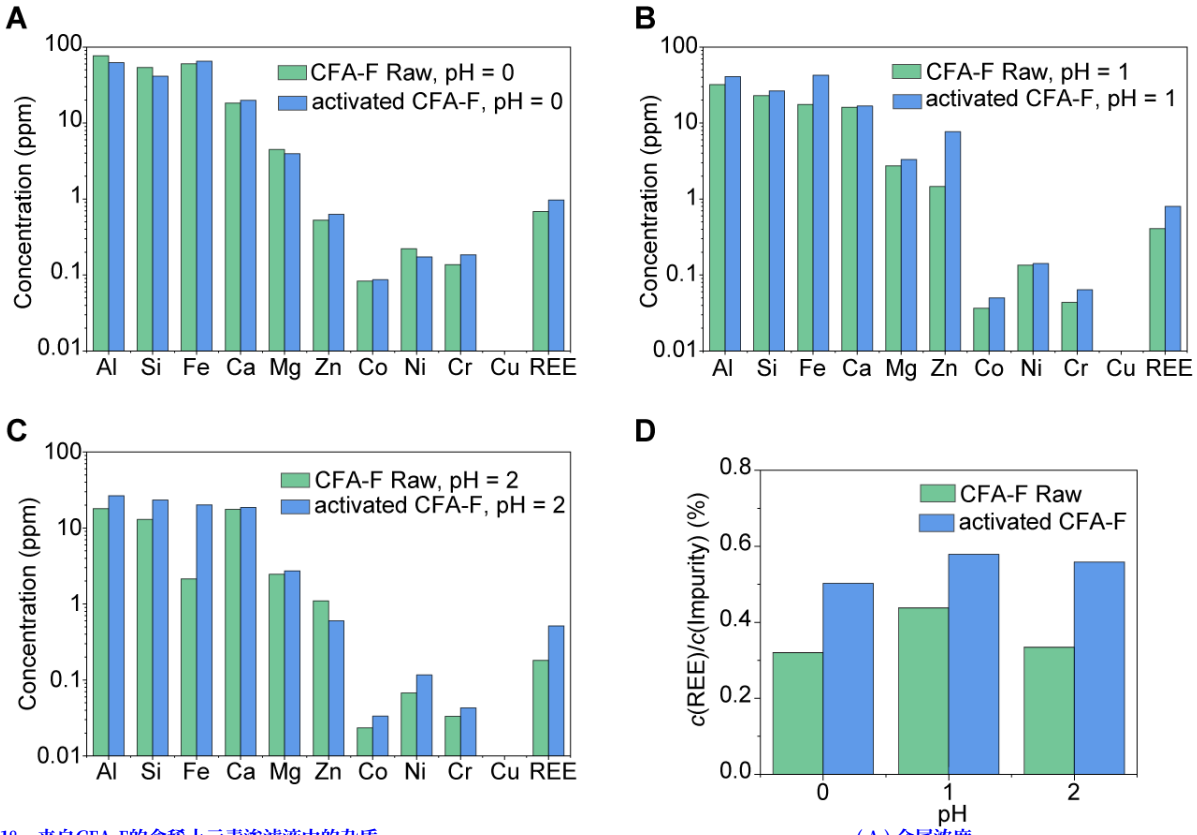

图S18。来自CFA-F的含稀土元素渗滤液中的杂质。（A）金属浓度

Fig. S18. Impurities in the REE-containing leachate from CFA-F. (**A**) Concentrations of metal impurities and REE in the leachate from CFA-F raw materials and activated CFA-F (1 M HCl, 85 °C). (**B**) Concentrations of metal impurities and REE in the leachate from CFA-F raw materials and activated CFA-F (0.1 M HCl, 85 °C). (**C**) Concentration of metal impurities and REE in the leachate from CFA-F raw materials and activated CFA-F (0.01 M HCl, 85 °C). (**D**) The ratio of REE content and metal impurities content in the leachate from CFA-F raw materials and activated CFA-F in leachant with different pH.

CFA-F原料和活化CFA-F（1 M HCl，85 ° C）渗滤液中的杂质和稀土元素。（B）CFA-F原料和活化CFA-F（0.1 M HCl，85 ° C）渗滤液中金属杂质和稀土元素的浓度。（C）CFA-F原料和活化CFA-F（0.01 M HCl，85 ° C）渗滤液中金属杂质和稀土元素的浓度。（D）研究了不同pH值的CFA-F原料渗滤液和活化CFA-F渗滤液中稀土元素含量和金属杂质含量的比值。

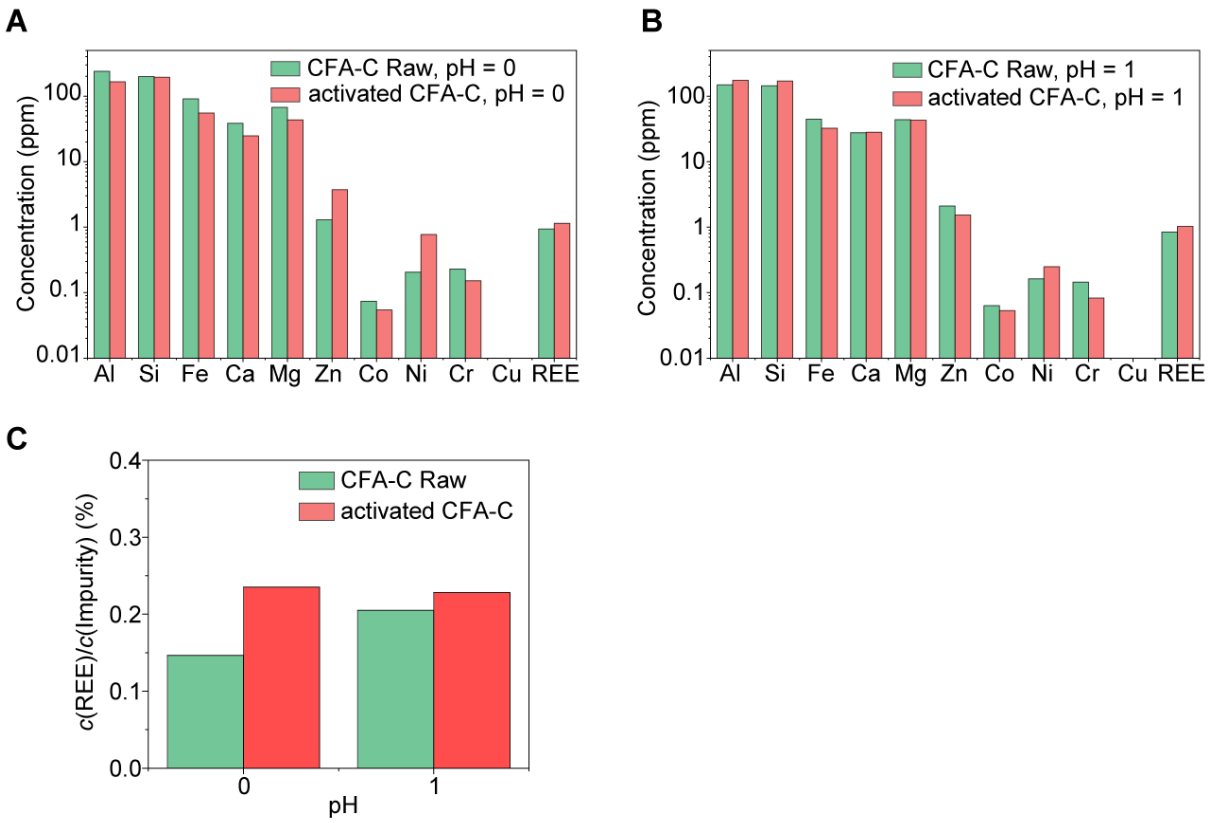

图S19。来自CFA-C的含稀土元素渗滤液中的杂质。（A）金属浓度CFA-C原料和活化CFA-C（1 M HCl，85 ° C）渗滤液中的杂质和稀土元素。（B）CFA-F原料和活化CFA-C（0.1 M HCl，85 ° C）渗滤液中金属杂质和稀土元素的浓度。（C）研究了不同pH值的CFA-C原料渗滤液和活化CFA-C渗滤液中稀土元素含量和杂质含量的比值。

Fig. S19. Impurities in the REE-containing leachate from CFA-C. (A) Concentrations of metal impurities and REE in the leachate from CFA-C raw materials and activated CFA-C (1 M HCl, 85 °C). **(B)** Concentrations of metal impurities and REE in the leachate from CFA-F raw materials and activated CFA-C (0.1 M HCl, 85 °C). **(C)** The ratio of REE content and impurities content in the leachate from CFA-C raw materials and activated CFA-C in leachant with different pH.

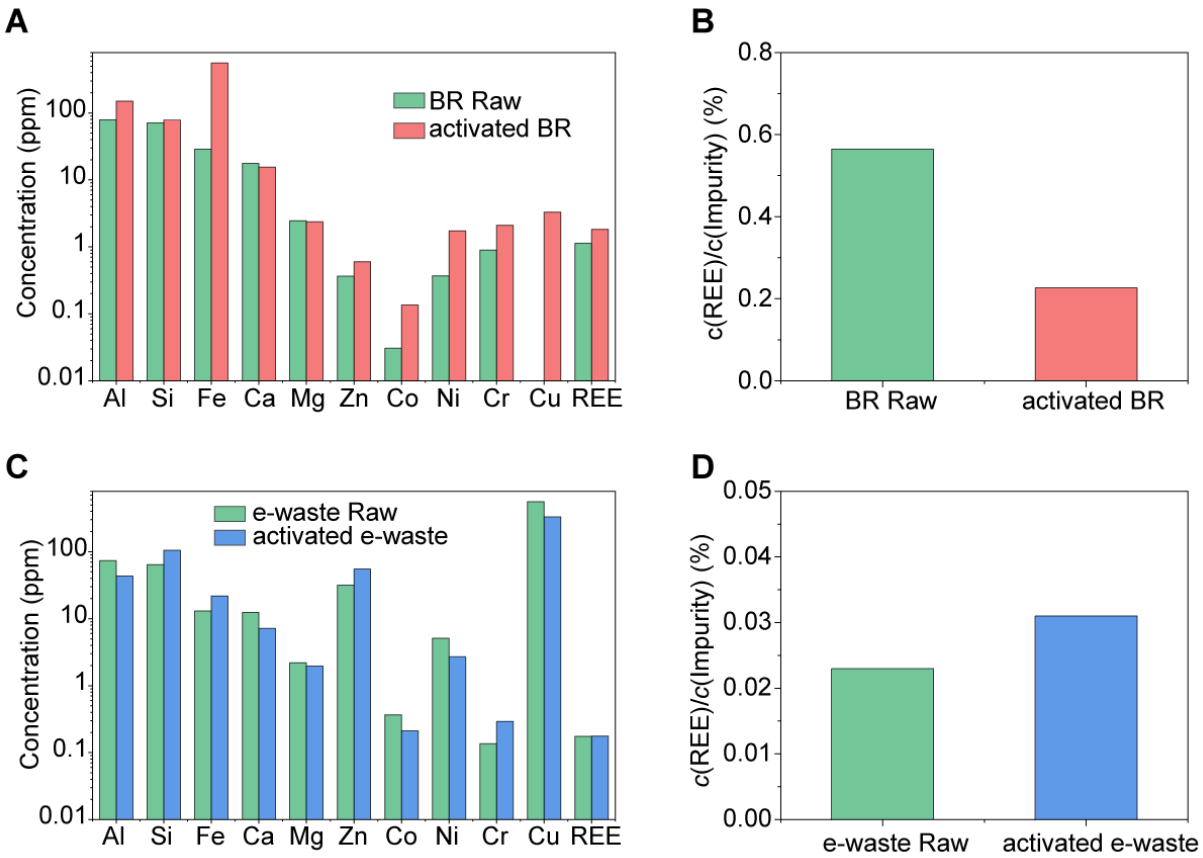

图S20。BR和电子垃圾中含有稀土元素的渗滤液中的杂质。（A）浓度

Fig. S20. Impurities in the REE-containing leachate from BR and e-waste. (**A**) Concentrations of metal impurities and REE in the leachate from BR raw materials and activated BR (0.5 M HNO_3, 85 °C). (**B**) The ratio of REE content and impurities content in the leachate from BR raw materials and activated BR. (**C**) Concentrations of metal impurities and REE in the leachate from e-waste raw materials and activated e-waste (1 M HCl, 85 °C). (**D**) The ratio of REE content and impurities content in the leachate from e-waste raw materials and activated e-waste.

BR原料和活性BR（0.5 M HNO3，（B）BR原料和活性BR渗滤液中稀土元素含量和杂质含量的比值。（C）电子废物原料和活化电子废物（1 M HCl，85 ° C）渗滤液中金属杂质和稀土元素的浓度。（D）电子垃圾原料和活化电子垃圾渗滤液中稀土元素含量和杂质含量的比率。

表S1。 二次废物活化的FJH参数。

Table S1. The FJH parameters for activation of secondary wastes.

前体质量 Precursors	比率 Mass Ratio	大量 Mass (mg)	反对 Resistance (Ω)	电压 Voltage (V)	时间 Time (s)	FJH后的质量 Mass after FJH (mg)
CFA-F:CB	2:1	200	1.0	50	1	190
CFA-F:CB	2:1	200	1.0	80	1	138
CFA-F:CB	2:1	200	1.0	100	1	115
CFA-F:CB	2:1	200	1.0	120	1	157
CFA-F:CB	2:1	200	1.0	150	1	88
CFA-C:CB	2:1	200	1.0	120	1	182
BR:CB	2:1	200	1.2	50	1	190
BR:CB	2:1	200	1.2	80	1	174
BR:CB	2:1	200	1.2	100	1	162
BR:CB	2:1	200	1.2	120	1	159
BR:CB	2:1	200	1.2	150	1	152
PCB:CB	2:1	200	1.0	50	1	162
PCB:CB	2:1	200	2.0	100	1	185
PCB:CB	2:1	200	2.0	120	1	98

表S2。代表性稀土磷酸盐的热分解温度。

Table S2. Thermal decomposition temperature of representative REE phosphates.

材料 Material	反应 Reaction	H(kJ mol-1) ΔH (kJ mol^{-1})	S(J mol-1 K-1) ΔS (J mol^{-1} K^{-1})	温度(°C) Temp (°C)
$LaPO_4$	$LaPO_4 = 1/2La_2O_3 + PO_2 + 1/4O_2$	817.65	260.45	2866
$CePO_4$	$CePO_4 = 1/2Ce_2O_3 + PO_2 + 1/4O_2$	785.8	256.3	2793
$PrPO_4$	$PrPO_4 = 1/2Pr_2O_3 + PO_2 + 1/4O_2$	798.8	269.8	2688
$NdPO_4$	$NdPO_4 = 1/2Nd_2O_3 + PO_2 + 1/4O_2$	780.85	262.1	2706
$SmPO_4$	$SmPO_4 = 1/2Sm_2O_3 + PO_2 + 1/4O_2$	774.3	256.5	2746
$EuPO_4$	$EuPO_4 = 1/2Eu_2O_3 + PO_2 + 1/4O_2$	765.0	266.7	2595
$GdPO_4$	$GdPO_4 = 1/2Gd_2O_3 + PO_2 + 1/4O_2$	766.4	253.9	2745

注：REEPO4=1/2REE2O3+PO2+1/4O2的分解反应用于所有稀土磷酸盐(30)。

Note: The decomposition reaction, $REEPO_4 = 1/2REE_2O_3 + PO_2 + 1/4O_2$, is used for all REE phosphates (*30*). The standard molar enthalpies and standard molar entropies of REE phosphates 稀土磷酸盐的标准摩尔焓和标准摩尔熵来自文献(62)，稀土氧化物、PO2和O2的这些常数来自CRC物理和化学手册(63)。 are from the literature (*62*), and these constants of REE oxides, PO_2, and O_2 are from the CRC Handbook of Physics and Chemistry (*63*).

表S3。25 ° C下稀土金属、氧化物和磷酸盐溶解反应的吉布斯自由能变化和溶解度积常数（Ksp）。

Table S3. Gibbs free energy change and solubility product constants (K_{sp}) of REE metals, oxides, and phosphates dissolution reactions at 25 °C.

材料反应

Materials	Reaction	ΔG	$Log_{10}K_{sp}$
Sc	$Sc + 3H^+ = Sc^{3+} + 3/2H_2$	-614.2 kJ mol^{-1}	107.61
Sc_2O_3	$1/2Sc_2O_3 + 3H^+ = Sc^{3+} + 3/2H_2O$	-32.61 kJ mol^{-1}	5.71
$ScPO_4$	$ScPO_4 = Sc^{3+} + PO_4^{3-}$	---	-26.96
Y	$Y + 3H^+ = Y^{3+} + 3/2H_2$	-693.8 kJ mol^{-1}	121.56
Y_2O_3	$1/2Y_2O_3 + 3H^+ = Y^{3+} + 3/2H_2O$	-141.19 kJ mol^{-1}	24.74
YPO_4	$YPO_4 = Y^{3+} + PO_4^{3-}$	---	-25.02
La	$La + 3H^+ = La^{3+} + 3/2H_2$	-683.7 kJ mol^{-1}	119.79
La_2O_3	$1/2La_2O_3 + 3H^+ = La^{3+} + 3/2H_2O$	-186.49 kJ mol^{-1}	32.67
$LaPO_4$	$LaPO_4 = La^{3+} + PO_4^{3-}$	---	-25.7
Ce	$Ce + 3H^+ = Ce^{3+} + 3/2H_2$	-672 kJ mol^{-1}	117.74
Ce_2O_3	$1/2Ce_2O_3 + 3H^+ = Ce^{3+} + 3/2H_2O$	-174.59 kJ mol^{-1}	30.59
$CePO_4$	$CePO_4 = Ce^{3+} + PO_4^{3-}$	---	-26.2
Pr	$Pr + 3H^+ = Pr^{3+} + 3/2H_2$	-679.1 kJ mol^{-1}	118.98
Pr_2O_3	$1/2Pr_2O_3 + 3H^+ = Pr^{3+} + 3/2H_2O$	-174.89 kJ mol^{-1}	30.64
$PrPO_4$	$PrPO_4 = Pr^{3+} + PO_4^{3-}$	---	-26.4
Nd	$Nd + 3H^+ = Nd^{3+} + 3/2H_2$	-671.6 kJ mol^{-1}	117.67
Nd_2O_3	$1/2Nd_2O_3 + 3H^+ = Nd^{3+} + 3/2H_2O$	-166.89 kJ mol^{-1}	29.24
$NdPO_4$	$NdPO_4 = Nd^{3+} + PO_4^{3-}$	---	-26.2
Sm	$Sm + 3H^+ = Sm^{3+} + 3/2H_2$	-666.6 kJ mol^{-1}	116.79
Sm_2O_3	$1/2Sm_2O_3 + 3H^+ = Sm^{3+} + 3/2H_2O$	-154.99 kJ mol^{-1}	27.16
$SmPO_4$	$SmPO_4 = Sm^{3+} + PO_4^{3-}$	---	-26.1
Eu	$Eu + 3H^+ = Eu^{3+} + 3/2H_2$	-574.1 kJ mol^{-1}	100.58
Eu_2O_3	$1/2Eu_2O_3 + 3H^+ = Eu^{3+} + 3/2H_2O$	-151.39 kJ mol^{-1}	26.52
$EuPO_4$	$EuPO_4 = Eu^{3+} + PO_4^{3-}$	---	-25.9
Gd	$Gd + 3H^+ = Gd^{3+} + 3/2H_2$	-661 kJ mol^{-1}	115.81
Gd_2O_3	$1/2Gd_2O_3 + 3H^+ = Gd^{3+} + 3/2H_2O$	-134.79 kJ mol^{-1}	23.62
$GdPO_4$	$GdPO_4 = Gd^{3+} + PO_4^{3-}$	---	-25.6
Tb	$Tb + 3H^+ = Tb^{3+} + 3/2H_2$	-651.9 kJ mol^{-1}	114.21
Tb_2O_3	$1/2Tb_2O_3 + 3H^+ = Tb^{3+} + 3/2H_2O$	-119.19 kJ mol^{-1}	20.88
$TbPO_4$	$TbPO_4 = Tb^{3+} + PO_4^{3-}$	---	-25.3
Dy	$Dy + 3H^+ = Dy^{3+} + 3/2H_2$	-665 kJ mol^{-1}	116.51
Dy_2O_3	$1/2Dy_2O_3 + 3H^+ = Dy^{3+} + 3/2H_2O$	-134.94 kJ mol^{-1}	23.64
$DyPO_4$	$DyPO_4 = Dy^{3+} + PO_4^{3-}$	---	-25.1
Ho	$Ho + 3H^+ = Ho^{3+} + 3/2H_2$	-673.7 kJ mol^{-1}	118.03
Ho_2O_3	$1/2Ho_2O_3 + 3H^+ = Ho^{3+} + 3/2H_2O$	-133.84 kJ mol^{-1}	23.45
$HoPO_4$	$HoPO_4 = Ho^{3+} + PO_4^{3-}$	---	-25.0
Er	$Er + 3H^+ = Er^{3+} + 3/2H_2$	-669.1 kJ mol^{-1}	117.23
Er_2O_3	$1/2Er_2O_3 + 3H^+ = Er^{3+} + 3/2H_2O$	-120.44 kJ mol^{-1}	21.10
$ErPO_4$	$ErPO_4 = Er^{3+} + PO_4^{3-}$	---	-25.1
Tm	$Tm + 3H^+ = Tm^{3+} + 3/2H_2$	-662 kJ mol^{-1}	115.98
Tm_2O_3	$1/2Tm_2O_3 + 3H^+ = Tm^{3+} + 3/2H_2O$	-120.44 kJ mol^{-1}	21.10
$TmPO_4$	$TmPO_4 = Tm^{3+} + PO_4^{3-}$	---	-25.0

连续表
Continuing table

材料反应 Materials	Reaction	ΔG	$Log_{10}K_{sp}$
Yb	$Yb + 3H^+ = Yb^{3+} + 3/2H_2$	-644 kJ mol^{-1}	112.83
Yb_2O_3	$1/2Yb_2O_3 + 3H^+ = Yb^{3+} + 3/2H_2O$	-136.34 kJ mol^{-1}	23.89
$YbPO_4$	$YbPO_4 = Yb^{3+} + PO_4^{3-}$	---	-24.8
Lu	$Lu + 3H^+ = Lu^{3+} + 3/2H_2$	-628 kJ mol^{-1}	110.03
Lu_2O_3	$1/2Lu_2O_3 + 3H^+ = Lu^{3+} + 3/2H_2O$	-89.19 kJ mol^{-1}	15.63
$LuPO_4$	$LuPO_4 = Lu^{3+} + PO_4^{3-}$	---	-24.7

注：对于稀土金属，log10Ksp值是根据CRC物理和化学手册(63)中的形成常数自由能计算得出的。

Note: For REE metals, the $log_{10}K_{sp}$ values are calculated from the free energy of formation constants in the CRC Handbook of Physics and Chemistry (*63*). 对于稀土氧化物，根据NBS热力学性质表(64)中报告的形成常数自由能计算log10Ksp值。 For REE oxides, the $log_{10}K_{sp}$ values are calculated from the free energy of formation constants reported in the NBS tables of thermodynamic properties (*64*). 在NBS表中，Pr2O3、Gd2O3和Tb2O3没有形成自由能；对于这些氧化物，根据NBS表(64)中元素的生成焓和标准熵以及文献(65)中氧化物的标准熵计算log10Ksp值。 There is no free energy of formation for Pr_2O_3, Gd_2O_3, and Tb_2O_3 in the NBS table; for these oxides, the $log_{10}K_{sp}$ values are calculated based on the enthalpy of formation and standard entropy for element from NBS table (*64*), and standard entropy of the oxides from a literature (*65*). 对于稀土磷酸盐，文献中报道了ScPO4(66)和其他稀土磷酸盐(67)的log10Ksp值。 For REE phosphates, the $log_{10}K_{sp}$ values are reported in literatures for $ScPO_4$ (*66*) and other REE phosphates (*67*). 通常，稀土磷酸盐很难溶解，log10Ksp值在-24到-27之间。 Generally, the REE phosphates are hard to dissolve and have the $log_{10}K_{sp}$ values in the range of -24 to -27. 这些值明显小于稀土金属和稀土氧化物的值。 These values are significantly smaller than those of REE metals and REE oxides. 因此，稀土金属和稀土氧化物比磷酸稀土金属和稀土氧化物更容易被酸萃取。 As a result, REE metals and REE oxides are much more extractable by acid than the REE phosphate counterparts.

表S4。 La和Y的XPS峰拟合。

Table S4. The XPS peak fitting of La and Y.

样品 Samples	要素 Element	位置(eV)，峰 Position (eV), peak	化学状态，化学键 Chemical state, Chemical bond
La_2O_3	La	834.8, La $3d_{5/2}$	+3, La-O
		838.2，卫星 838.2, satellite	+3, La-O
FJH La之后的La2O3 La_2O_3 after FJH	La	834.8, La $3d_{5/2}$	+3, La-O
		836.0, La $3d_{5/2}$	0, La-La
		838.1，卫星 838.1, satellite	+3, La-O
		839.6，卫星 839.6, satellite	0, La-La
Y_2O_3	Y	157.4, Y $3d_{5/2}$	+3, Y-O
		159.4, Y $3d3_{/2}$	+3, Y-O
FJH Y后的Y2O3 Y_2O_3 after FJH	Y	156.4, Y $3d_{5/2}$	0, Y-Y
		157.5, Y $3d_{5/2}$	+3, Y-O
		158.5, Y $3d_{3/2}$	0, Y-Y
		159.6, Y $3d_{3/2}$	+3, Y-O